

The 't Hooft equation as a quantum spectral curve

David Vegh

*Centre for Theoretical Physics, Department of Physics and Astronomy
Queen Mary University of London, 327 Mile End Road, London E1 4NS, UK*

email: d.vegh@qmul.ac.uk

September 11, 2024

Abstract

In an attempt to establish a link between different quantization methods, I examine the massless 't Hooft equation, which governs meson bound state wavefunctions in 2d $SU(N)$ gauge theory in the large- N limit. The integral equation can also be obtained by lightcone quantizing a folded string in flat space. The folded string is a limiting case of a more general setup: a four-segmented string moving in AdS_3 . I compute its classical spectral curve by using celestial variables and planar bipartite graphs (on-shell diagrams/brane tilings). The adjugate of the Kasteleyn matrix vanishes at two special points, which ensures that the string segments form a closed loop in target space. The Hamiltonian takes on a Ruijsenaars-Schneider form and the phase space is a coadjoint $SL(2)$ orbit whose middle region has been removed. In AdS, the 't Hooft equation acquires an extra term, which has previously been proposed as an effective confining potential in QCD. After an integral transform, the equation can be inverted in terms of a finite difference equation. I show that this difference equation can be interpreted as the quantized (non-analytic) spectral curve of the string. I calculate the spectrum numerically, which interpolates between $M^2 = n(n+1)$ in the tensionless limit and 't Hooft's nearly linear Regge trajectory at infinite AdS radius.

Contents

1	Introduction	2
2	The folded string in AdS_2	4
3	Segmented strings in AdS_3	6
3.1	Celestial variables	7
3.2	The four-segmented string	9
4	Classical spectral curve	12
4.1	Spectral curve from celestial variables	12
4.2	Spectral curve from tiling variables	15
4.3	Squashing the four-segmented string	18
5	Hamiltonian mechanics	19
5.1	Canonical variables on the spectral curve	19
5.2	$\mathfrak{sl}(2)$ Ruijsenaars-Schneider Hamiltonian	20
5.3	Physical coordinates as level sets	22
5.4	Tiling variables vs. spectral curve coordinates	24
6	Quantum spectral curve	30
6.1	The 't Hooft equation	30
6.2	Canonical variables in flat space	31
6.3	Quantum spectral curve in flat space	34
6.4	Quantum spectral curve in AdS	36
7	Numerical spectrum	39
8	Discussion	42
A	Closing constraints and the adjugate Kasteleyn matrix	45

1 Introduction

Quantizing a classical system is not a straightforward procedure and the prescription can fail for several reasons. In general, it is difficult to find a Hilbert space and assign self-adjoint operators to the relevant observables. Operators typically do not commute, consequently an ordering ambiguity arises and various quantization schemes may be used to find a consistent quantum theory. Especially difficult is the quantization of constrained systems and systems with gauge redundancies. An example for such a system is the bosonic (Nambu-Goto) string on a general background. On highly symmetrical target spaces the worldsheet theory may be integrable—at least classically [1]. Two-dimensional integrable theories can oftentimes be discretized in an exact manner (so that both spatial and time directions are discrete), which renders the phase space finite dimensional. This motivates the study of discrete strings, in the hope that perhaps the quantization is under more control¹.

In the theory of integrability, Baxter’s T–Q equation [4, 5] plays a key role in various models. The equation is a finite difference equation² and in certain cases it can be interpreted as a quantized spectral curve. Recently, integrability techniques have been brought to bear on the AdS/CFT correspondence [9–11] in the planar limit. In the seminal paper [12] it was recognized that the one-loop spectrum of $\mathcal{N} = 4$ SYM is captured by an integrable spin chain. It was also discovered that superstrings on the dual $\text{AdS}_5 \times S^5$ background are classically integrable [13]. These results generated a great deal of interest, which culminated in the construction of the $\text{AdS}_5/\text{CFT}_4$ quantum spectral curve³ [16, 17] (see [18–20] for reviews of the subject).

The existing quantum spectral curve constructions are rather intricate due to the large symmetry groups. In this paper we will explore a much simpler system: a closed segmented string and make a first step towards comparing different approaches to quantization. The string under consideration is the folded string, which is depicted in Figure 1. It is composed of two massless particles connected by two identical string segments so that the string forms a (collapsed) closed loop in flat space. In a (1+1)-dimensional target space the system has a four-dimensional phase space, but the center-of-mass coordinates will decouple leaving us with a two-dimensional phase space. Note that fixing the number of particles in a relativistic quantum theory is dangerous as it generally leads to a broken Lorentz symmetry. Never-

¹Another motivation might come from the fact that some sort of discretization scheme is necessary when the string motion is simulated on a computer. String-like excitations can also appear in a statistical physics model that lives on a discrete lattice, which further motivates the study of discrete strings. See [2, 3] for earlier works on discrete strings.

²Finite difference equations also play an important role in other areas of physics, such as in the diffraction theory of waves incident on wedges or cones (see e.g. [6]), or in the quantization of a self-gravitating spherically symmetric dust shell in comoving coordinates [7, 8].

³Recently there have been proposals for the quantum spectral curve of $\text{AdS}_3 \times S^3 \times T^4$ [14, 15].

theless, by going to an infinite momentum frame one can deal with this issue and obtain a consistent quantum theory.

In order to compare the variables used in lightcone quantization with those used to parametrize the spectral curve, we first need to compute the spectral curve itself. Since the calculation in flat space is somewhat degenerate, we compute the curve in AdS_3 instead. We find a transformation between physical coordinates and the quasimomentum and the spectral parameter, denoted by p and u , respectively. The physical configuration space turns out to be the $|u| \geq 2g$ subset of the real line, where $g := L^2/(2\pi\alpha')$ is a constant and L is the AdS radius. By cutting out the unphysical $(-2g, +2g)$ region, and denoting the new coordinate by q , we obtain a non-analytic real spectral curve,

$$e^p + e^{-p} + 2 - \frac{M^2}{q^2 + 4g|q|} = 0, \quad (1)$$

where M is the energy of the string. We recall the derivation of the 't Hooft equation by lightcone quantizing the folded string and generalize it to the case of AdS. The only contribution coming from the curvature of the target space is an extra term in the equation. We find a canonical transformation between (p, u) and the lightcone variables, which (following [21]) enables us to invert the modified 't Hooft equation and obtain the difference equation,

$$Q(q+i) + Q(q-i) - 2Q(q) = -\frac{M^2}{q^2 + 4gq \coth(\pi q)} Q(q),$$

which is identified as the quantum version of the non-analytic spectral curve in (1).

The paper is organized as follows. In section 2 we discuss the folded string in AdS_3 . This is a one-dimensional example and its Hamiltonian can be computed in a straightforward way. The section closely follows section 4.3 in [22]. In section 3 we discuss more general segmented strings, in particular the four-segmented case, which will be at the center of our focus. The embedding into AdS_3 is described and the target space string energy is calculated. Section 4 discusses the spectral curve of the four-segmented string. The calculation of the curve is done in different ways: by using 2×2 Lax matrices containing (i) celestial and (ii) Möbius invariant tiling variables. In order to ensure that the string closes in the target space, certain “closing constraints” must be satisfied, which are discussed in some detail. Section 5 introduces canonical variables on the spectral curve and derives the $SL(2)$ Ruijsenaars-Schneider Hamiltonian for the four-segmented string. We discuss the transformation between various coordinates and compute their Poisson brackets. In section 6 we recall the derivation of the 't Hooft equation by lightcone quantizing the string and find the map between lightcone variables and spectral curve coordinates. We discuss the integral transform of the original 't Hooft equation along with its AdS counterpart. Section 7 provides details on the numerical calculation of the spectrum. In the appendix we point out a potentially interesting reformulation of the closing constraints in terms of the adjugate of the Kasteleyn matrix.

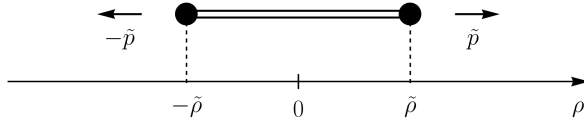


Figure 1: A folded “yo-yoing” string consists of two massless particles connected by two string segments. The particles move with the speed of light in AdS and bounce back when they reach maximum extension. The motion is periodic in time. The position and momentum of one of the particles is denoted by $\tilde{\rho}$ and \tilde{p} , respectively.

2 The folded string in AdS₂

Strings with longitudinal kink modes have been studied since the early days of string theory. These can be thought of as a set of particles connected by strings. For a non-comprehensive list of papers discussing strings with longitudinal degrees of freedom in flat space, we refer the reader to [23–26]. The idea of a folded string with several folds can be generalized to a d -dimensional anti-de Sitter (AdS _{d}) target space. In this section we will discuss the simplest folded string, which moves in AdS₂ and has two folds. The system can be depicted as two particles connected by two identical string segments as shown in Figure 1. In this section, we summarize the results of section 4.3 in [22], where the authors derived the spacetime Hamiltonian using a direct approach.

The action can be written as [27]

$$\mathcal{S}_{\text{string}} = -\frac{1}{4\pi\alpha'} \int_M d^2\sigma \sqrt{-h} h^{ab} \partial_a X^\mu \partial_b X^\nu G_{\mu\nu} + \int_{\partial M} d\xi \frac{1}{2\eta} \dot{X}^\mu \dot{X}^\nu G_{\mu\nu},$$

where M is the worldsheet and ∂M is its boundary. The endpoints carry momentum, which is taken into account by the second term. The worldsheet metric h_{ab} is determined by its equation of motion (up to a conformal factor). $\eta = \eta(\xi)$ is the einbein on the boundary worldline, parametrized by the coordinate ξ . The AdS₂ target space metric is given by

$$ds^2 = L^2(-\cosh^2 \rho d\tau^2 + d\rho^2),$$

where the domain of both coordinates is the entire real line. Following [22], we parametrize the worldsheet using the τ and ρ coordinates. For simplicity, we take a symmetric string configuration centered at $\rho = 0$ and parametrize the worldline of the endpoints using the coordinate $\xi = \tau$. The location of one of the endpoints is denoted by $\tilde{\rho}(\tau)$ and it will be the dynamical variable in the following. Thus, ρ runs from $-|\tilde{\rho}|$ to $+|\tilde{\rho}|$, covering half of

the worldsheet, i.e. one of the string segments in Figure 1. The string Lagrangian can be computed explicitly [22]

$$\mathcal{L} = -\frac{2L^2}{\pi\alpha'} \int_0^{|\tilde{\rho}|} d\rho \cosh \rho + \frac{L^2}{\eta} (-\cosh^2 \tilde{\rho} + \dot{\tilde{\rho}}^2) = -\frac{2L^2}{\pi\alpha'} \sinh |\tilde{\rho}| + \frac{L^2}{\eta} (-\cosh^2 \tilde{\rho} + \dot{\tilde{\rho}}^2), \quad (2)$$

Performing the Legendre transformation and eliminating η gives the Hamiltonian in terms of the location of one of the endpoints $\tilde{\rho}(\tau) \in (-\infty, \infty)$ and the conjugate momentum $\tilde{p}(\tau)$ [22]

$$\tilde{H}(\tilde{p}, \tilde{\rho}) = \tilde{p}\dot{\tilde{\rho}} - \mathcal{L} = |\tilde{p}| \cosh \tilde{\rho} + \frac{2L^2}{\pi\alpha'} \sinh |\tilde{\rho}|, \quad (3)$$

and we have $\{\tilde{\rho}, \tilde{p}\} = 1$. Note that in the $\tilde{\rho} \ll 1$ flat space limit, (3) reduces to the ‘‘zigzag’’ Hamiltonian [28–30], which for two particles is given by

$$\tilde{H}_{\text{flat}} = |\tilde{p}| + \frac{2L^2}{\pi\alpha'} |\tilde{\rho}| = |\tilde{p}| + 4g|\tilde{\rho}|, \quad (4)$$

where we have introduced the constant

$$g := \frac{L^2}{2\pi\alpha'}.$$

The authors of [22] also write down the WKB quantization condition,

$$\frac{\mathcal{S}}{4} \equiv \int_0^{\tilde{\rho}_0} d\tilde{\rho} \tilde{p}(\tilde{\rho}) = \frac{\pi}{2} n,$$

where n is the quantum number and $\tilde{p}(\tilde{\rho})$ is obtained from the equation $\tilde{H} = M$ where M is the energy of the string in units of AdS radius. The integral limit $\tilde{\rho}_0$ is determined so that $\tilde{p}(\tilde{\rho}_0) = 0$. This yields

$$\int_0^{\tilde{\rho}_0} d\tilde{\rho} (M - 4g \sinh \tilde{\rho}) \operatorname{sech} \tilde{\rho} = \frac{\pi}{2} n. \quad (5)$$

For small $\tilde{\rho}_0$, we get the Regge trajectory for the physical mass m ,

$$(mL)^2 = M^2 = \frac{2L^2}{\alpha'} n = 4\pi g n. \quad (6)$$

On the other hand, for large $\tilde{\rho}_0$, eqn. (5) gives the scaling

$$M - n = \frac{8g}{\pi} \log n + \mathcal{O}(n^0). \quad (7)$$

As the authors of [22] note, this result is very similar to that of a rigidly rotating long string in higher-dimensional AdS [31], with the only difference being in the coefficient multiplying the logarithm.

As we will see in section 5, there are several alternative descriptions of this simple string system. The derivation relies on integrability, for which we need to recast the system into the appropriate language. This will be the topic of the next section.

3 Segmented strings in AdS₃

The folded string is somewhat complicated, because it contains both particles and string segments. In this section we consider a less singular configuration, from which the folded string can be recovered as a limiting case. First, we develop the general case and then in section 3.2 we specialize to the system of interest: the string with four segments.

The target space will be taken to be three-dimensional AdS space⁴ and the classical string motion will extremize the Nambu-Goto action. An important property of the Nambu-Goto string in AdS is that it is described by an integrable field theory [1]. Such theories can often be discretized in an exact fashion. This means that a discrete integrable model can be embedded into the field theory and discrete solutions correspond to special continuous solutions. Furthermore, the field theory can be recovered by taking a small lattice spacing limit of the discrete model⁵. Here we will use a particular discretization of the bosonic string—the *segmented string* [22, 33–41]. The embeddings are piecewise linear, i.e. the string is built from several joint segments. An example is displayed in Figure 2 (left). The worldsheet of a string segment is a patch of an AdS₂ subspace inside AdS₃. Such segments are characterized by constant normal vectors. Adjacent segments are joined by *kinks*, which move with the speed of light. This is necessary, otherwise the string tension would immediately bend the string near the joints and the segmentedness property would be destroyed. Thus, kink worldlines form a quad lattice on the worldsheet, which is shown in Figure 2 (middle).

For practical calculations we will use the split signature $\mathbb{R}^{2,2}$ ambient space, in which the points of AdS₃ lie on a hyperboloid,

$$Y \cdot Y \equiv -Y_{-1}^2 - Y_0^2 + Y_1^2 + Y_2^2 = -L^2, \quad Y \in \mathbb{R}^{2,2}.$$

In sections 3 and 4 we set $L = 1$ for simplicity (unless otherwise stated).

As seen in Figure 2, each AdS₂ patch on the worldsheet is bounded by four kink lines. If three of the vertices of the patch are known, then the fourth one can be calculated via a *reflection formula* [34, 35]. If $Y^{(i)}$ denote the ordered vertices around the patch as in Figure 2 (right), then for instance the third vertex can be computed by the formula

$$Y^{(3)} = -Y^{(1)} - 4 \frac{Y^{(2)} + Y^{(4)}}{(Y^{(2)} + Y^{(4)})^2}. \quad (8)$$

Similarly, one can express $Y^{(1)}, Y^{(2)}, Y^{(4)}$ from the other three vertices. If appropriate initial conditions are known, the reflection formula enables us to calculate the entire string embedding, which will extremize the Nambu-Goto action.

⁴The reason for taking AdS as a target space is (i) to make contact with the AdS/CFT correspondence [9–11] and (ii) because certain quantities (e.g. the normal vector) are more covariant in AdS.

⁵See e.g. [32] for many discrete integrable models and their continuous counterparts.

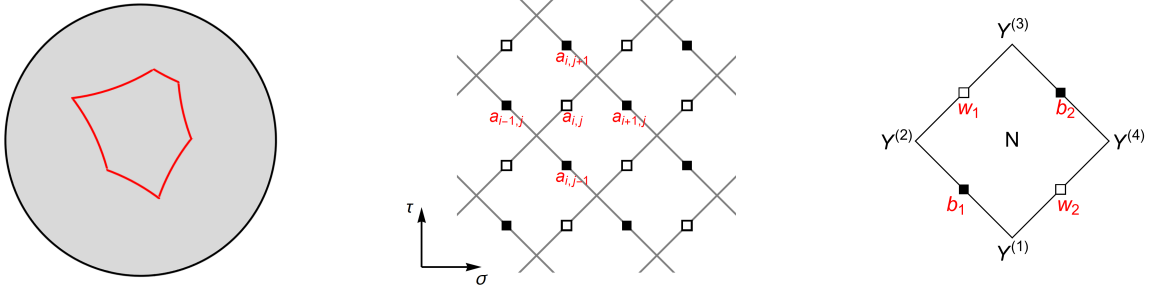


Figure 2: *Left:* Segmented string on a timeslice of global AdS_3 . The example contains six kinks. *Middle:* A small patch of the worldsheet of a segmented string. Kinks (black lines) travel at $\pm 45^\circ$ angles, forming a lattice on the worldsheet. The velocity of a kink is characterized by a null tangent vector in the ambient space $\mathbb{R}^{2,2}$. The corresponding a_{ij} celestial variables can be written on the edges, indicated by black and white squares depending on edge orientation. Here i and j correspond to discretized σ and τ coordinates, respectively. For a closed string, $a_{ij} = a_{i+n,j}$, where n is the number of string segments. *Right:* Zooming in on a single AdS_2 patch on the worldsheet.

An alternative description uses normal vectors instead of kink vertices. Let $Y(\sigma^+, \sigma^-)$ denote the embedding function. The normal vector is defined by

$$N_a \propto \epsilon_{abcd} Y^b \partial_+ Y^c \partial_- Y^d \quad \text{such that} \quad N^2 = 1.$$

An elementary AdS_2 patch has a constant normal vector. Time evolution of the normal vectors on the worldsheet is governed by the expression

$$N^{(3)} = -N^{(1)} + 4 \frac{N^{(2)} + N^{(4)}}{(N^{(2)} + N^{(4)})^2}$$

where the $N^{(i)}$ are the normal vectors of four adjacent patches. This equation differs from eqn. (8) only in a sign and can also be used to compute the time evolution of the embedding as was originally done in [33].

3.1 Celestial variables

In practice, the reflection formula is numerically unstable: tiny errors that inevitably arise on a computer (due to storing real numbers up to certain number of digits) get amplified over time. We will now describe a way around this problem by using embedding variables that take values on the celestial torus [34].

Let us consider the kink ‘velocity’ vectors in Figure 2 (middle). These are defined to be the difference vectors between adjacent vertices. For instance, in Figure 2 (right) the four

kink velocity vectors are given by $X = Y^{(2)} - Y^{(1)}$, $Y^{(4)} - Y^{(1)}$, $Y^{(3)} - Y^{(4)}$ and $Y^{(3)} - Y^{(2)}$, respectively. These are all null vectors, therefore by means of the spinor-helicity formalism, we can decompose them into products of (real) two-component $\mathbb{R}^{2,2}$ spinors. The Nambu-Goto action (the area of the worldsheet) can be written in terms of these spinors. Due to its special form, the discrete action only depends on the ratio of the two spinor components. These ratios can be expressed using the velocity vector components X_i as

$$a = \frac{X_{-1} + X_2}{X_0 + X_1}, \quad \tilde{a} = \frac{X_{-1} - X_2}{X_0 + X_1}, \quad (9)$$

for the left and right spinors, respectively. For instance, if $X = Y^{(2)} - Y^{(1)}$, then (9) gives b_1 , which is shown in Figure 2 (right) and \tilde{b}_1 (suppressed in the figure). These variables are dubbed *celestial variables*. Since they correspond to kink worldlines, the discrete field $a_{ij} \in \mathbb{R}$ lives on a square lattice on the worldsheet. Here $i \in \mathbb{Z}$ and $j \in \mathbb{Z}$ correspond to discretized σ and τ coordinates, respectively. For a closed string, $a_{ij} = a_{i+n,j}$ and $\tilde{a}_{ij} = \tilde{a}_{i+n,j}$, where n is the number of string segments. This lattice is indicated by black and white boxes in Figure 2 (middle) and the coloring depends on which way the kink moves. Using the fact that the kink velocity vectors around a patch (with appropriate signs) must add up to zero, one can eliminate the \tilde{a} variables from the action. Finally, one obtains the equation of motion of a discrete-time Toda lattice,

$$\frac{1}{a_{ij} - a_{i,j+1}} + \frac{1}{a_{ij} - a_{i,j-1}} = \frac{1}{a_{ij} - a_{i+1,j}} + \frac{1}{a_{ij} - a_{i-1,j}}. \quad (10)$$

The full embedding can be recovered from the celestial variables (up to a global $SL(2)$ transformation) [34]. In what follows, it will be useful to introduce the ‘reflection matrix,’ which depends on two adjacent celestial variables b and w [39]

$$\mathcal{R}_{b,w} = \frac{1}{b-w} \begin{pmatrix} 0 & bw+1 & bw-1 & -b-w \\ -1-bw & 0 & b+w & bw-1 \\ -1+bw & b+w & 0 & -1-bw \\ -b-w & bw-1 & bw+1 & 0 \end{pmatrix}. \quad (11)$$

Let us consider the patch on the right of Figure 2. The normal vector N can be computed from $Y^{(2)}$ simply by letting the reflection matrix act on it,

$$N = \mathcal{R}_{b_1,w_1} Y^{(2)}.$$

Furthermore, from the normal vector N and the celestial variables, all four $Y^{(i)}$ vertices can be computed. We have,

$$Y^{(1)} = \mathcal{R}_{b_1,w_2} N, \quad Y^{(3)} = \mathcal{R}_{b_2,w_1} N, \quad Y^{(4)} = \mathcal{R}_{b_2,w_2} N.$$

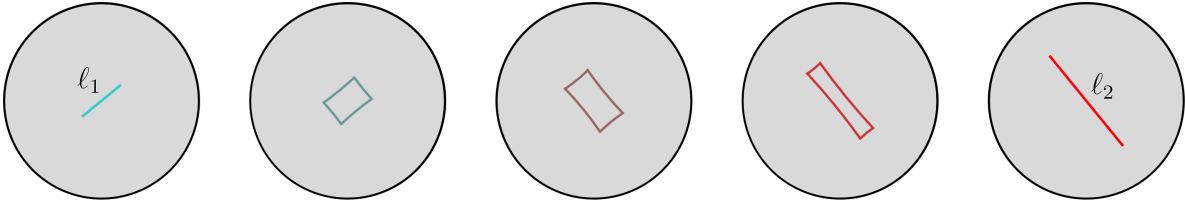


Figure 3: Snapshots of a closed string in global AdS_3 . The motion is periodic in time. The string oscillates between the leftmost and rightmost configurations, which are characterized by their lengths ℓ_1 and ℓ_2 .

By repeatedly applying the reflection matrix on the position and normal vectors, all the other patch vertices can be computed, which finally fixes the string embedding. Note that only information from the a_{ij} variables has been used (the \tilde{a}_{ij} variables are not independent).

Initial conditions for the time evolution can be given by specifying two adjacent rows, e.g. $a_{i,0}$ and $a_{i,1}$ for all i . In the case of closed strings it is important to note that these two rows cannot be arbitrary real numbers. Constraints arise from the fact that the string must form a closed loop. The a_{ij} variables are trivially periodic (they are chosen that way). However, the suppressed \tilde{a}_{ij} variables must also be periodic. Since \tilde{a}_{ij} can be computed from a_{ij} in a non-local way, this condition imposes three real constraints on a_{ij} . The constraints can be expressed using either the reflection matrix (11), or in terms of the 2×2 Lax matrices [40], which will be discussed in detail in section 4.

3.2 The four-segmented string

In this section we discuss in detail the simplest closed segmented string, which consists of four elementary segments. The folded string from the previous section will turn out to be a special case. Figure 3 displays the motion of a generic four-segmented string in its rest frame. The snapshots are timeslices of global AdS_3 , separated by fixed timesteps. The motion is periodic and the shape of the string gradually changes from the interval on the left (short blue line) to the interval on the right (long red line) and then back again *ad infinitum*. In the rest frame, the shape of any four-segmented string can be characterized by the two length scales corresponding to the intervals. In the following, we will parametrize these lengths by two constants r_1 and r_2 . We will later relate these parameters to the geodesic lengths ℓ_1, ℓ_2 .

The worldsheet of the four-segmented string is shown in Figure 4. Since the string is closed, the horizontal direction is periodic and the two dashed lines must be identified. N_{ab} denote the normal vectors of the individual patches. P and Q denote two spacetime

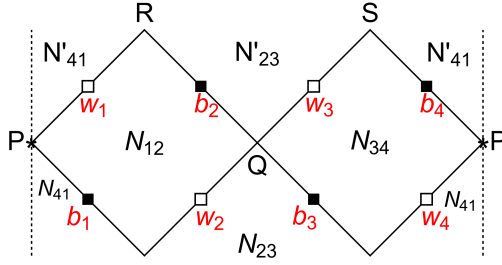


Figure 4: Periodic worldsheet of the four-segmented string. Solid black lines indicate kink worldlines. $N_{12}, N_{23}, N'_{23}, N_{34}, N_{41}, N'_{41}$ label the normal vectors of the corresponding AdS_2 patches. b_i and w_j are celestial variables. P, Q, R, S are vertices (i.e. kinks collide there).

“events” where kinks on the string collide. The symmetric segmented string with $r_1 = r_2$ was described in [22] and the corresponding normal vectors were computed in [40]. We now generalize these findings by considering the general case. We will set the AdS radius $L = 1$.

Let us consider the normal vectors,

$$\begin{aligned}
N_{12} &= \left(r, -\frac{r_2}{r_1}\sqrt{1+r^2}, 0, +\frac{d}{r_1} \right), \\
N_{23} &= \left(r, +\frac{r_1}{r_2}\sqrt{1+r^2}, -\frac{d}{r_2}, 0 \right), \\
N_{34} &= \left(r, -\frac{r_2}{r_1}\sqrt{1+r^2}, 0, -\frac{d}{r_1} \right), \\
N_{41} &= \left(r, +\frac{r_1}{r_2}\sqrt{1+r^2}, +\frac{d}{r_2}, 0 \right).
\end{aligned} \tag{12}$$

where we defined the constants r and d ,

$$r := \frac{\sqrt{2}r_1r_2}{\sqrt{r_1^2 + r_2^2}}, \quad d := \sqrt{r_1^2 + r_2^2 + 2r_1^2r_2^2}. \tag{13}$$

It is easy to check that the normal vectors are unit vectors. Furthermore, the scalar product of pairs of normal vectors corresponding to adjacent segments satisfy

$$N_{12}N_{23} = N_{23}N_{34} = N_{34}N_{41} = N_{41}N_{12} = 1,$$

which ensures that the kinks between the segments move with the speed of light [33].

The spacetime energy of the string can be computed by a straightforward integration of the energy density as in section 4 of [22]. We would like to do this integral from the point P

to Q . We have $PN_{12} = PN_{41} = PN_{34} = QN_{12} = QN_{23} = QN_{34} = 0$, $P^2 = Q^2 = -1$, from which we obtain

$$\begin{aligned} P &= \left(\sqrt{1+r^2}, \frac{\sqrt{2}r_1^2}{\sqrt{r_1^2+r_2^2}}, +\sqrt{2}r_1, 0 \right), \\ Q &= \left(\sqrt{1+r^2}, \frac{\sqrt{2}r_1^2}{\sqrt{r_1^2+r_2^2}}, -\sqrt{2}r_1, 0 \right). \end{aligned}$$

As is well-known, the geodesic distance ℓ_1 between P and Q can be computed from the dot-product,

$$\cosh \ell_1 = -P \cdot Q = 1 + 4r_1^2, \quad (14)$$

which is the actual length of the string in the first plot in Figure 3. Similarly,

$$\cosh \ell_2 = -R \cdot S = 1 + 4r_2^2 \quad (15)$$

gives the length of the string in the last plot.

If τ denotes global AdS time, then at the P and Q points $\tan \tau = \frac{d}{\sqrt{2}r_1^2}$ and for the $\tau - \tau$ component of the spacetime energy-momentum tensor we get (in units of $2\pi\alpha'$),

$$P_\tau^\tau = \frac{d}{r_1},$$

The energy of the string is

$$M = 2 \left| \int_{Y_P^1}^{Y_Q^1} dY^1 P_\tau^\tau \right|.$$

In order to take into account the other segment (from Q back to P), we have multiplied the integral by two. The integral limits are the third components of the P and Q vectors: $Y_P^1 = \sqrt{2}r_1$ and $Y_Q^1 = -\sqrt{2}r_1$ [22]. Finally we get

$$M(r_1, r_2) = 4\sqrt{2}d = 4\sqrt{2}\sqrt{r_1^2 + r_2^2 + 2r_1^2r_2^2}. \quad (16)$$

If either r_1 or r_2 vanishes, then the entire motion of the four-segmented string is constrained to an AdS_2 subspace. In this case, the shape of the string is just a straight line and two of the normal vectors in (12) have diverging components. The corresponding segments are vanishingly small and they move with the speed of light. In this limit they can be regarded as massless particles, connected by the other two extended string segments as shown in Figure 1. Finally, the celestial variables can also be determined. Since we have a folded worldsheet, some of the kinks in Figure 4 travel on identical worldlines. Thus, the corresponding celestial variables are also equal,

$$b_3 = w_2, \quad w_3 = b_2, \quad w_4 = b_1, \quad b_4 = w_1.$$

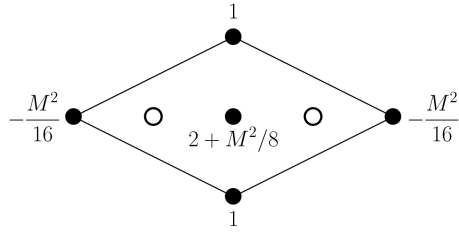


Figure 5: Newton polygon of the spectral curve (22) of the four-segmented string ($g = 1$). All non-zero coefficients are written next to the lattice points (empty circles indicate zeroes).

4 Classical spectral curve

In an integrable system the spectral curve is an important invariant, which encodes conserved quantities. In this section we compute the spectral curve of the four-segmented string. Although this system has only one degree of freedom (and thus it is somewhat trivial from an integrability perspective), the calculation will still be useful for it enables us to identify a natural pair of canonically conjugate variables and compute the spacetime Hamiltonian in a straightforward way, complementing the discussion in section 2.

The spectral curve can be computed either by multiplying 2×2 Lax matrices, or by computing the determinant of the dressed adjacency matrix—the Kasteleyn matrix—of a relevant bipartite graph. In the following, we will discuss these methods.

4.1 Spectral curve from celestial variables

The elementary 2×2 Lax matrix for a path starting on a kink collision vertex and ending on an adjacent AdS_2 patch is given by [40]

$$\Omega_{b,w}(x) = \frac{1}{(b-w)\sqrt{x}} \begin{pmatrix} bx - w & bw(1-x) \\ x - 1 & b - wx \end{pmatrix} \quad (17)$$

Here x is a spectral parameter⁶ and b, w are two celestial variables corresponding to kink worldlines which collide in a vertex. The matrix describes the parallel transport between the vertex and the patch. For instance, in Figure 2 (right), Ω_{b_1, w_1} would correspond to the path from $Y^{(2)}$ to N . Here the symbol N stands for both the patch and its normal vector⁷.

⁶Note that [40] defines the Lax matrix in terms of the spectral parameter $\zeta \equiv \sqrt{x}$.

⁷Note that there is a ‘duality’ between AdS_3 and the space of normal vectors.

Starting at point P and going around the string, the monodromy is given by

$$\Omega_P(x) = \Omega_{b_4, w_4}^{-1} \Omega_{b_3, w_3} \Omega_{b_2, w_2}^{-1} \Omega_{b_1, w_1}. \quad (18)$$

It should be mentioned that the monodromy does depend on the starting point (and changes by conjugation if we start elsewhere), but we will suppress the label as it will not be important in what follows.

In order for the string to form a closed loop in target space, the variables must satisfy *closing constraints*. In terms of the Ω matrix, the constraints are given by [40]

$$\Omega(x = -1) = \mathbb{1}. \quad (19)$$

This equation will be referred to as the celestial closing constraint. Note that $\Omega(x = 1) = \mathbb{1}$ is trivially true, implying that the celestial variables a_{ij} are already periodic ($a_{i+4, j} = a_{ij}$). Eqn. (19) says that the string embedding is periodic, therefore \tilde{a}_{ij} must also be periodic. Since $\det \Omega = 1$, (19) constrains three out of the eight celestial variables. Three more variables can be fixed by means of an $SL(2)$ isometry transformation, which acts as a Möbius transformation on celestial variables. The remaining two variables span the two-dimensional phase space of the string.

The spectral curve is given by

$$\det(y\mathbb{1} + \Omega(x)) = 0. \quad (20)$$

The expression is quite complicated in terms of the celestial variables, especially when (19) is used to restrict three of them. Although celestial variables do transform under $SL(2)$, the spectral curve remains invariant. Hence, the variables must appear in certain Möbius-invariant combinations in the equation defining the curve.

The internal energy of the string M can be computed by expanding $\text{tr} \Omega^n$ at special points, but it can also be computed directly as follows. Figure 4 shows all the relevant celestial variables. Our goal is to determine r_1 and r_2 , which enter the formula (16) for the energy. Let us denote the components of the vertex Q by

$$Q = (q_{-1}, q_0, q_1, q_2).$$

From Q , we can compute the normal vectors of neighboring patches,

$$N_{12} = \mathcal{R}_{b_2, w_2} Q, \quad N_{34} = \mathcal{R}_{b_3, w_3} Q.$$

Another application of the reflection matrix gives the point

$$P = \mathcal{R}_{b_1, w_1} N_{12}.$$

Now using (14) and the fact that $Q^2 = -1$, we obtain

$$r_1^2 = \frac{(b_2 - b_1)(w_1 - w_2)}{2(b_1 - w_1)(b_2 - w_2)}.$$

Note that the components of Q have dropped out of the final expression. In order to compute r_2 , we proceed to compute the points

$$R = \mathcal{R}_{b_2, w_1} N_{12}, \quad S = \mathcal{R}_{b_4, w_3} N_{34}.$$

Using (15) and $Q^2 = -1$, we obtain

$$r_2^2 = \frac{(b_3 - b_4)(w_1 - w_2)(b_2 - w_3)^2}{2(b_2 - w_1)(b_2 - w_2)(b_3 - w_3)(w_3 - b_4)}.$$

This result is slightly more complicated than the one for r_1 , because R and S lie a bit farther away from the two rows of celestial variables than P and Q . Let us now fix three of the variables, say w_3, b_4, w_4 , by imposing (19). We get [41]

$$\begin{aligned} w_3 &= \frac{b_1 w_1 (b_3 - w_2) + b_2 w_2 (w_1 - b_3) + b_1 b_2 (w_2 - w_1)}{b_1 (b_3 - w_1) + b_3 (w_1 - w_2) + b_2 (w_2 - b_3)}, \\ b_4 &= \frac{b_1 b_2 (b_3 + w_1 - w_2) + w_1 w_2 (b_3 - b_2) + b_1 w_1 (w_2 - 2b_3)}{b_1 (b_2 - b_3) - w_1 b_3 + b_2 (b_3 - 2w_2) + w_2 (w_1 + b_3)}, \\ w_4 &= \frac{w_1 b_2 (b_3 - w_2) + b_1 (b_2 (w_1 - w_2) + w_2 (w_1 + b_3) - 2w_1 b_3)}{b_2 (w_1 + b_3 - 2w_2) + b_1 (w_2 - b_3) + b_3 (w_2 - w_1)}. \end{aligned} \tag{21}$$

Using these expressions and eqn. (16) for $M(r_1, r_2)$, it is easy to see that the spectral curve can be rewritten in the invariant form,

$$y + y^{-1} - \frac{M^2}{16}(x^2 + x^{-2}) + 2 + \frac{M^2}{8} = 0. \tag{22}$$

Finally, all the explicit celestial dependence is gone from the equation. The Newton polygon of the curve is shown in Figure 5.

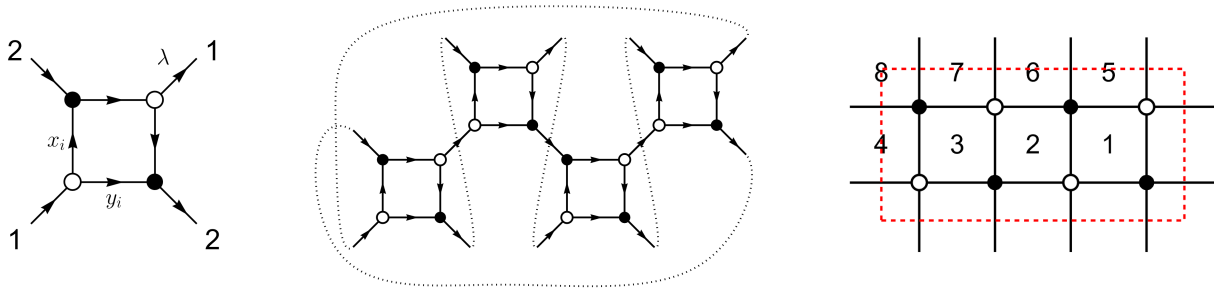


Figure 6: *Left*: Elementary network (or on-shell diagram). *Middle*: The four-segmented string requires gluing four elementary networks in a periodic way. *Right*: Collapsing nodes of the same color gives the brane tiling: a doubly periodic bipartite graph.

4.2 Spectral curve from tiling variables

The spectral curve of segmented strings can also be computed using an alternative technique based on *on-shell diagrams* or *brane tilings*⁸. This technique was first described by the author in [41]. The objects in question are doubly periodic planar bipartite graphs, i.e. they can be drawn on the surface of a torus without crossing edges. An example is shown in Figure 6 (right), where the fundamental domain is indicated by a dashed rectangle.

Natural variables associated to the tiling are Möbius-invariant and we can relate them to celestial variables by taking cross-ratios of the latter. We will use the notation

$$(a, b; c, d) \equiv \frac{(a-b)(c-d)}{(a-d)(b-c)}.$$

We adopt the following definition of the tiling variables x_{ij} and y_{ij} [41, 47],

$$x_{ij} := -(a_{i+1,j+1}, a_{i+2,j}; a_{i+1,j}, a_{ij}), \quad (23)$$

$$x_{ij} + y_{ij} := -(a_{i+1,j+1}, a_{i+2,j+1}; a_{i+1,j}, a_{ij}), \quad (24)$$

Discrete time evolution (i.e. $j \rightarrow j+1$) is given by the formulas [48]

$$x_{i,j+1} = x_{i-1,j} \frac{x_{ij} + y_{ij}}{x_{i-1,j} + y_{i-1,j}}, \quad y_{i,j+1} = y_{i,j} \frac{x_{i+1,j} + y_{i+1,j}}{x_{ij} + y_{ij}}. \quad (25)$$

The expressions (23)-(24) contain celestial variables from rows j and $j+1$. For the four-segmented string, these two rows are shown in Figure 4. Henceforth, we will suppress the

⁸The name “brane tiling” comes from the study of D-branes probing non-compact toric Calabi-Yau spaces. In this context, the graphs indicate brane configurations in a certain duality frame. For a non-comprehensive list of papers on the subject, see [42–45]. For on-shell diagrams, see [46].

index j . Altogether we have defined eight tiling variables: x_i and y_i for $i = 1 \dots 4$, but they are not independent due to the closing constraints.

The tiling can be constructed from elementary building blocks. The elementary network is depicted in Figure 6 (left)⁹. It contains two black and two right nodes and directed links between them. The direction of the edges are defined such that white nodes have two outgoing links, while black nodes only have one. We associate weights to the edges as shown in the Figure. In addition to x_i, y_i , we have introduced a spectral parameter λ , which takes into account that the outgoing links are shifted on the right-hand side of the diagram.

We define the weight of a directed path as the product of its edge weights. The “boundary measurement matrix” of the elementary network is a 2×2 matrix. Its rows and columns are labeled by ingoing and outgoing links and the elements are the sums of weights of all directed paths connecting the two endpoints. It is easily computed [47]

$$B_i(\lambda) = \begin{pmatrix} -\lambda x_i & x_i + y_i \\ -\lambda & 1 \end{pmatrix}. \quad (26)$$

Unlike (17), this matrix is Möbius-invariant. The Lax matrix is the normalized boundary measurement matrix,

$$L_i := \frac{B_i}{\sqrt{\det B_i}},$$

such that $\det L_i = 1$. The Lax monodromy is given by the product of Lax matrices¹⁰,

$$L(\lambda) = L_1 L_2 L_3 L_4. \quad (27)$$

The spectral parameter λ can be identified with x from the previous section. The closing constraints can be written as¹¹

$$L(1) = \mathbb{1}, \quad L(-1) = \mathbb{1}. \quad (28)$$

These equations are Möbius-invariant. An interpretation of the equations is that the underlying celestial variables must be periodic. If for given tiling variables x_i and y_i the constraints are not satisfied, then one can still locally assign celestial variables so that (23) and (24) are true, but these celestial variables will suffer an $SL(2)$ monodromy as we go around the string. The requirement that the monodromy is trivial for both a_{ij} and \tilde{a}_{ij} reduces the number of independent variables by six¹². Solving the constraints gives

$$x_1 = x_3 = -X^{-1}, \quad x_2 = x_4 = X, \quad y_1 = y_3 = X^{-1} - X - Y, \quad y_2 = y_4 = Y, \quad (29)$$

⁹In the context of on-shell diagrams, this is a four-particle tree-amplitude [46].

¹⁰Note that the order of multiplication is reversed compared to (18).

¹¹The general N -segmented case will be discussed elsewhere.

¹²In the previous section, we arrived at a two-dimensional phase space in an asymmetric way. There $\Omega(x)$ explicitly contained a_{ij} , which were assumed to be periodic from the start. The closing constraint (19) eliminated three celestial variables, and a further reduction came by considering Möbius-invariance.

where we parametrized the 2d phase space by X and Y . A straightforward calculation shows that these relations follow from (23) and (24) by plugging in (21). From (25) we get the discrete time step,

$$X \mapsto \frac{1}{X}, \quad Y \mapsto -Y. \quad (30)$$

Moreover, an explicit calculation reveals the following relationship between tiling variables and radii,

$$X = -r_1 r_2 \frac{\sqrt{2}}{d}, \quad Y = -\frac{r_2}{r_1} \frac{1}{d\sqrt{2}}, \quad (31)$$

where we used the constant d defined in (13). This result can be obtained in a straightforward (but lengthy) way by considering the normal vectors in (12), then calculating the celestial variables in a frame where they are not singular, and then finally evaluating x_i and y_i on the first discrete time slice. Since tiling variables are Möbius-invariant, the result is true in any frame. We can express the radii,

$$r_1^2 = \frac{x_2}{2y_2} = \frac{X}{2Y}, \quad r_2^2 = \frac{x_2}{2y_1} = \frac{X}{2(X^{-1} - X - Y)}, \quad (32)$$

It is important to note that since $r_1, r_2 \geq 0$, the quantities on the RHS of both of the equations are also non-negative. It is easy to see that the discrete time step (30) simultaneously flips the sign of both of these quantities.

For the internal energy of the string we get

$$M = 4g \left(\frac{X}{Y(1 - X^2 - XY)} \right)^{\frac{1}{2}}, \quad (33)$$

where we have reinstated the dependence on the AdS radius through the constant g . The discussion below (32) implies that the internal energy is a real number. Moreover, it is invariant under discrete time steps. Using the relations in (32), it is easy to show that (33) is equal to $M(r_1, r_2)$ in (16) (for $g = 1$).

Finally, the spectral curve of the four-segmented string is given by

$$\det(y\mathbb{1} + L(x)) = 0. \quad (34)$$

Using (29) and (33), the spectral curve can again be cast in the form of (22).

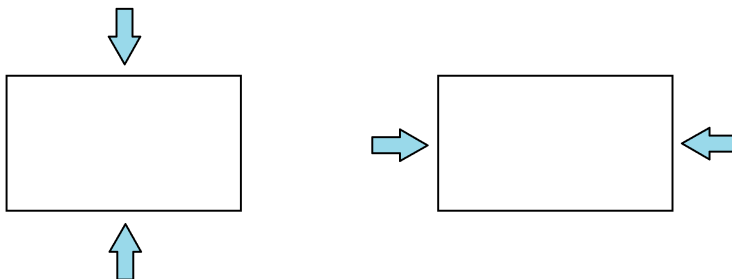


Figure 7: The four-segmented string can be squashed into a one-dimensional folded string by sending either $r_1 \rightarrow 0$ or $r_2 \rightarrow 0$ while keeping M fixed. The spectral curve is blind to this squashing procedure.

4.3 Squashing the four-segmented string

A remarkable fact is that the spectral curve does not contain complete information about the shape of the segmented string. Although the string can be characterized in an $SO(2, 2)$ -invariant way by two non-negative parameters, namely r_1 and r_2 as we discussed in section 3.2, the spectral curve in (35) only depends on these numbers via the energy function $M(r_1, r_2)$, which was given in (16). This means that we cannot unambiguously reconstruct the string embedding based purely on information contained in the spectral curve. In fact, we can squash the string embedding by sending either r_1 or r_2 all the way to zero while keeping the energy fixed. The resulting string will have the same phase space as far as the internal (Möbius-invariant) degrees of freedom are concerned. Moreover, since the squashed string moves in an AdS_2 subspace, it is nothing but the folded string, which was described in section 2.

As a consequence, we will be able to find a canonical transformation between the phase spaces of the four-segmented string in AdS_3 and the folded string in AdS_2 . (Note that there are two choices for this map, because as Figure 7 shows, we can set either r_1 or r_2 to zero.) Henceforth we will exploit this result and, with a slight abuse of language (and geometry), we will talk about a folded string and particles at its endpoints even when we discuss the four-segmented string.

5 Hamiltonian mechanics

5.1 Canonical variables on the spectral curve

In the previous section we have obtained the spectral curve of the four-segmented string (see Figure 3). It is given by the equation

$$y + y^{-1} - \frac{M^2}{16}(x^2 + x^{-2}) + 2 + \frac{M^2}{8} = 0, \quad (35)$$

where M is the energy of the string, while x and y are spectral coordinates. The spectral curve corresponds to both the discrete model, whose equation of motion is given in (10), as well as the continuous-time sigma model, in which the segmented string is a somewhat singular solution [40].

In order to make contact with commonly used spectral parameters in the literature, let us define the Zhukovskiy variable χ (which we will only use here)

$$x =: \frac{\chi - 1}{\chi + 1}, \quad (36)$$

and then immediately switch to another spectral parameter u by taking a further *Zhukovskiy transformation*,

$$u := (\chi + \chi^{-1})g, \quad (37)$$

where we have introduced the constant g . After a corresponding rescaling of the energy $M \rightarrow \frac{M}{g}$, the spectral curve (35) becomes

$$y + y^{-1} + 2 - \frac{M^2}{u^2 - 4g^2} = 0. \quad (38)$$

Let us define the quasimomentum p by setting $y = e^p$. Based on results for the smooth string¹³, we expect that p and u form a pair of canonically conjugate variables: $\{u, p\} = 1$. They can be thought of as natural “separated” variables, even though the system has only one degree of freedom¹⁴. The quasimomentum is obtained from the spectral curve

$$p(u) = \cosh^{-1} \left[\frac{M^2}{2(u^2 - 4g^2)} - 1 \right] = 2 \cosh^{-1} \left[\frac{M}{2\sqrt{u^2 - 4g^2}} \right]. \quad (39)$$

Similarly to section 2, the system is quantized semiclassically by imposing the condition

$$\frac{\mathcal{S}}{4} \equiv \int_{2g}^{u_0} du p(u) = \frac{\pi}{2} n$$

¹³See [49] and the thesis [50] for the case where the string is embedded into $\mathbb{R} \times S^3$.

¹⁴For a review of separation of variables, see [51] and references therein.

for the quarter period. The upper limit of the integration is the turning point defined by $p(u_0) = 0$, which gives $u_0 = \sqrt{\frac{M^2}{4} + 4g^2}$. The integral can be evaluated with the result

$$\mathcal{S} = \frac{\pi M}{2} - 2g \log \left(\frac{M^2}{16} + g^2 \right) + 4g \log g - M \tan^{-1} \frac{4g}{M},$$

and from this expression the results in section 2 can be derived.

5.2 $\mathfrak{sl}(2)$ Ruijsenaars-Schneider Hamiltonian

Using the expression for the quasimomentum in (39), we can express the spacetime Hamiltonian from $p(M, u) = p$. We get

$$H(p, u) = M = 2 \cosh \left(\frac{p}{2} \right) \sqrt{u^2 - 4g^2}. \quad (40)$$

Here p and u are canonically conjugate variables. The Hamiltonian resembles that of the Ruijsenaars-Schneider (RS) model [52], which is a one-parameter deformation of the Calogero-Moser model and it is relativistic in a certain sense [53]. Analogously to the original RS model we can define the momentum and boost generators,

$$P := 2 \sinh \left(\frac{p}{2} \right) \sqrt{u^2 - 4g^2}, \quad B := -2u.$$

Together they form an $\mathfrak{sl}(2)$ algebra,

$$\{H, P\} = -B, \quad \{H, B\} = P, \quad \{P, B\} = H.$$

We also have

$$-H^2 + P^2 + B^2 = 16g^2.$$

As an aside, we note that the above expressions for the generators naturally show up as components of an $\mathbb{R}^{2,1}$ embedding of AdS_2 , if we parametrize it using ‘‘Schwarzschild’’ coordinates,

$$(X_{-1}, X_0, X_1) = (B(p, u), P(p, u), H(p, u)),$$

where p and u are identified with Schwarzschild time and radius, respectively. Time evolution generated by H corresponds to rotation in the (X_{-1}, X_0) plane, which is simply global time evolution in AdS_2 . As global time passes, at $u = \pm 2g$ we cross the horizon, which is where p diverges. This corresponds to the collision of the two particles in Figure 1 (or the collision of kinks in the four-segmented case). The phase space is an orbifold of AdS_2 in which the ‘‘black hole’’ horizons of both exterior regions are identified with the ‘‘white hole’’ horizons of the other region.

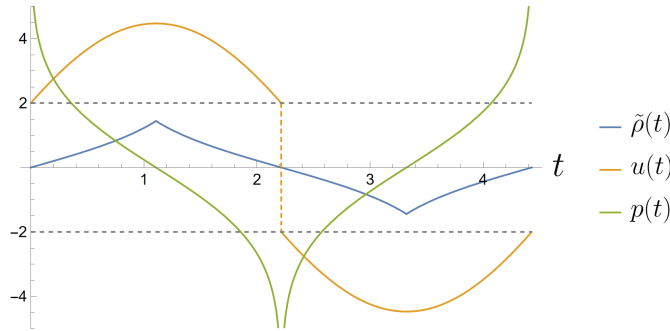


Figure 8: Time evolution of dynamical variables of the folded string in AdS_2 (with $g = 1$). Here $\tilde{\rho}$ is the physical position of one of the particles at the end of the string (see Figure 1), while p and u denote spectral curve coordinates on the phase space. The particles collide at $u = \pm 2g$ where $|p| \rightarrow \infty$. These two points in phase space are therefore identified.

In order to understand the “meaning” of p and u and examine which regions are physically allowed, we need to find an explicit canonical transformation to physical coordinates. Assuming p and u are real, $H(p, u)$ can be transformed into the Hamiltonian (3) by setting $g = L^2/(2\pi\alpha')$, $\tau = t$, and applying the following transformation (found by trial and error),

$$\tilde{p}(p, u) = P = 2 \sinh\left(\frac{p}{2}\right) \sqrt{u^2 - 4g^2}, \quad \tilde{\rho}(p, u) = 2 \tanh^{-1} \left(e^{-\frac{|p|}{2}} \sqrt{\frac{|u| - 2g}{|u| + 2g}} \right) \text{sgn } u. \quad (41)$$

Physical values of u satisfy $|u| \geq 2g$. At $u = \pm 2g$, we get $\tilde{\rho} = 0$ and the two particles collide. The momentum p diverges as seen in Figure 8. Since $u = \pm 2g$ correspond to the same string configuration, they should be identified. The above transformation is non-analytic both at these points and at the turning points where p vanishes. On the segmented string these correspond to kink collision events. It is straightforward to check that away from these one-dimensional lines in the phase space, (41) is in fact a canonical transformation.

Figure 8 shows the time evolution of various dynamical variables for an yo-yoing string. Let us shift the time coordinate so that the string is pointlike at $t = 0$. Then, $\tilde{\rho}$ reaches its maximal value at

$$t_{\max} = \tan^{-1} \frac{M}{4g}.$$

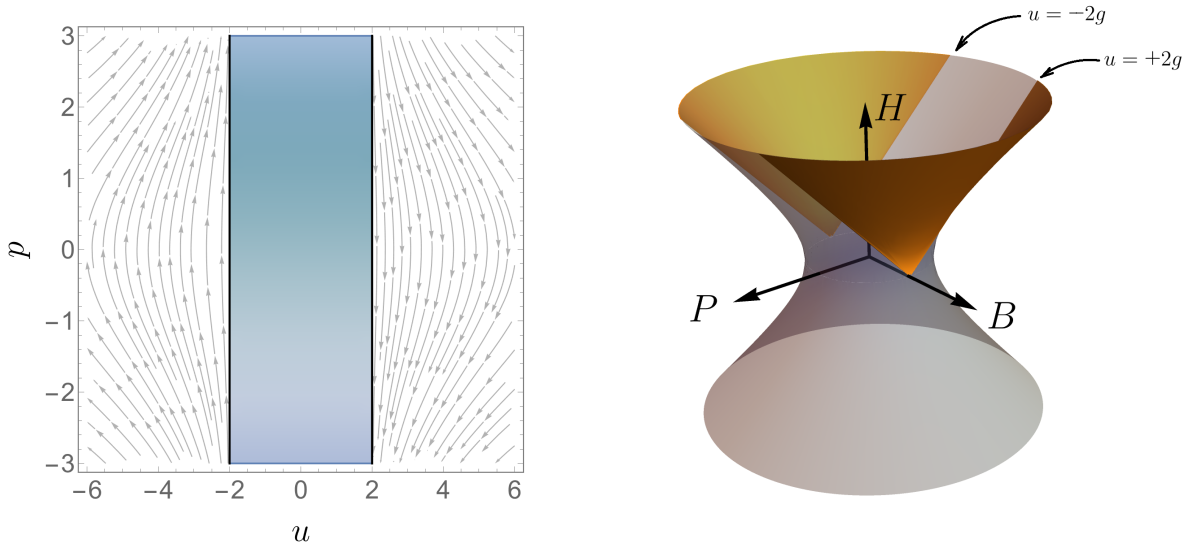


Figure 9: *Left:* Phase space and Hamiltonian flow of the four-segmented string in terms of natural variables p and u (for $g = 1$). The region $|u| < 2g$ is not part of the phase space. *Right:* The phase space (gold regions) in (H, P, B) space. The two regions should be glued together along their v-shaped boundaries at $u = \pm 2g$. The Hamiltonian is bounded from below. The Hamiltonian flow generates rigid rotation about the H axis.

The period of oscillation is $4t_{\max}$. We have

$$u(t) = \begin{cases} 2g \cos t + \frac{M}{2} \sin t & (0 < t < 2t_{\max}) \\ -2g \cos(t - 2t_{\max}) - \frac{M}{2} \sin(t - 2t_{\max}) & (2t_{\max} < t < 4t_{\max}) \end{cases}$$

$$p(t) = 2 \sinh^{-1} \frac{u'(t)}{\sqrt{u(t)^2 - 4g^2}}.$$

At $t = 2t_{\max}$, $u(t)$ jumps from $+2g$ to $-2g$ and the momentum diverges.

5.3 Physical coordinates as level sets

Where does the transformation (41) come from? Here we make an observation, which might elucidate the origin of the map. Let us recall how the RS model describes the motion of solitonic particles in several (1+1)-dimensional integrable models, such as the sine-Gordon theory. First, we define functions over a two-dimensional domain by acting on the initial values with both time evolution and then the evolution generated by P ,

$$(p(t, t'), u(t, t')) := e^{t'P} e^{tH}(p(0, 0), u(0, 0)).$$

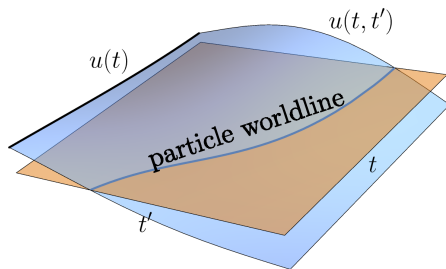


Figure 10: Computing soliton position from Ruijsenaars-Schneider variable $u(t)$ (schematic picture). The flows generated by H and P are parametrized by t and t' , respectively. The particle worldline $\tilde{\rho}(t) = -t'(t)$ is given implicitly by the level set $u(t, t') = 2g \operatorname{sgn} u(t, 0)$.

The second flow is parametrized by the t' coordinate. It should be mentioned that unlike in the original RS model, here P does not commute with the Hamiltonian.

The flow generated by P is given by

$$\frac{du}{dt'} = \{u, P\} = \cosh\left(\frac{p}{2}\right) \sqrt{u^2 - 4g^2}, \quad \frac{dp}{dt'} = \{p, P\} = -\frac{2u \sinh\left(\frac{p}{2}\right)}{\sqrt{u^2 - 4g^2}}.$$

RS coordinates do not directly denote soliton positions. Instead, soliton trajectories are defined by level sets of the u function. In the case of the string $u = \pm 2g$ are special points, because they correspond to kink collisions (this is where the folded string collapses to a point). Thus, the most natural level set seems to be

$$\boxed{u(t, t') = \pm 2g}, \quad (42)$$

which should be considered as an equation for $t'(t)$. We choose the sign in (42) so that it coincides with $\operatorname{sgn} u(t, 0)$. Let us now consider the phase space point $(p(t, 0), u(t, 0))$ at a give time. The flow starting from this point and generated by P can be integrated. For the u component we get

$$u(t, t') = u(t, 0) \cosh t' + \cosh\left(\frac{p(t, 0)}{2}\right) \sqrt{u(t, 0)^2 - 4g^2} \sinh t'.$$

Along this flow, P is constant. Now we can compute the flow time t' that is needed to satisfy the level set condition (42). Note that since $\frac{du}{dt'} \geq 0$ always, for $u > 2g$ ($u < -2g$) we will have to evolve backwards (forwards) in t' . The final result is precisely (41) with $\tilde{\rho}(t) = -t'(t)$.

In summary, the transformation from spectral curve coordinates (p, u) to physical coordinates $(\tilde{p}, \tilde{\rho})$ is similar to the map that connects RS particle positions to the positions of solitons in an associated two-dimensional field theory.

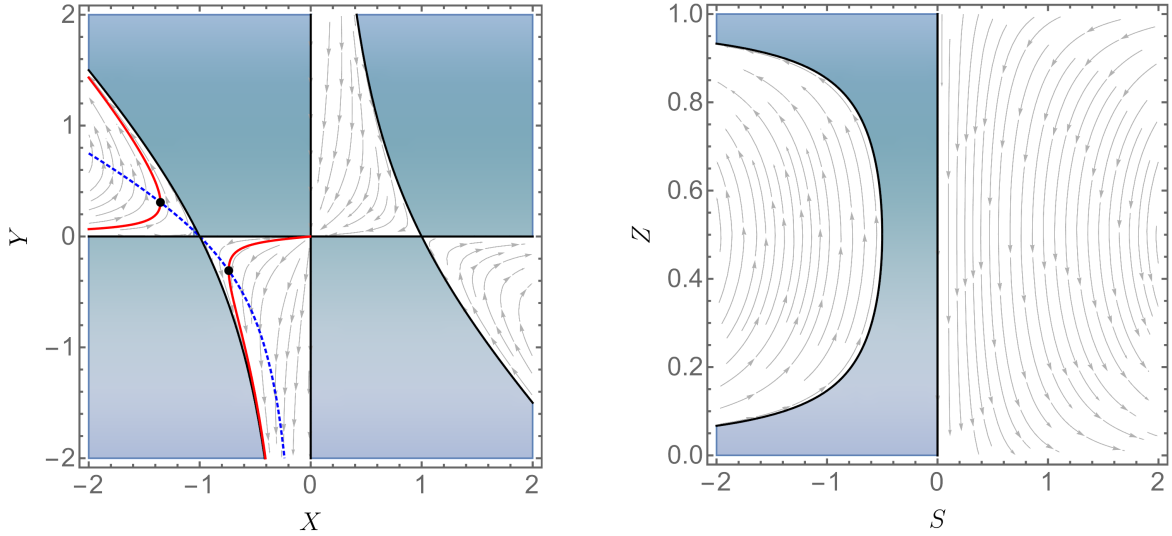


Figure 11: *Left:* Phase space and Hamiltonian flow of the four-segmented string in terms of X and Y (with $g = 1$). Excluded regions where $M^2 < 0$ are shown in blue. The variable X is always negative and the sign of Y is indefinite. In the continuum model, the state of the system evolves according to the stream plot. The trajectory of a particular solution is shown as a solid red line. The discrete model is embedded into the continuum theory and its dynamical variables only take specific values. For instance, in the case of $r_1 = r_2$ the allowed values are indicated by a blue dotted line and the system oscillates between two points (shown by two black dots for the example) connected by (30). *Right:* Phase space and Hamiltonian flow of the four-segmented string in terms of Z and S of the “first map” (with $g = \frac{1}{32}$). The “second map” has a similar, mirrored diagram.

5.4 Tiling variables vs. spectral curve coordinates

Now that we have found a canonical transformation between the spectral curve coordinates (p, u) and the physical coordinates $(\tilde{p}, \tilde{\rho})$, let us proceed and find a map that connects the tiling coordinates (X, Y) to the other two pairs. Finding such a map is crucial, because it will let us calculate the Poisson brackets of (X, Y) . The Poisson structure together with the Hamiltonian (33) will allow us to reformulate the dynamics in terms of tilings variables.

Note that up until now the tiling variables have described geometrical properties of the segmented string via (23)-(24). In the following, they will be understood to be dynamical variables of the continuum time model $X(t)$ and $Y(t)$. The change of variables that we are seeking can be obtained from the Baker-Akhiezer function and the “magical prescription” for the separation of variables [51]. We obtain two distinct maps as follows.

First map

Let us consider the 2×2 Lax monodromy matrix (27) and plug in the solution of the closing constraint (29). From $L_{12}(x) = 0$ we obtain the identification $X = x$. Then from $L_{22}(x) = e^{-p}$ we obtain two solutions for Y and pick the one that gives $H(X, Y) = H(p, u)$ (see (33) and (40)). For real coordinate values we get

$$X(p, u) = x = \sqrt{\frac{u-2g}{u+2g}}, \quad Y(p, u) = 2g \frac{\tanh\left(\frac{p}{2}\right) + 1}{\sqrt{u^2 - 4g^2}} \operatorname{sgn} u, \quad (43)$$

where the positive square root must be taken. The inverse transformations are given by

$$u(X, Y) = 2g \frac{1 + X^2}{1 - X^2}, \quad p(X, Y) = -2 \tanh^{-1} \left(\frac{1 - X^2 - 2XY}{1 - X^2} \right), \quad (44)$$

and they are invariant under the reflection $(X, Y) \rightarrow (-X, -Y)$.

Figure 11 (left) shows the two-dimensional phase space spanned by X and Y . The way the discrete-time model is embedded into the continuous-time model depends on r_1 and r_2 separately. For instance, if we plug $r_1 = r_2$ into (31), then we get the relationship $2XY + X^2 = 1$. This curve is indicated by a dashed blue line in the Figure. The discrete model undergoes discrete time steps according to (30) and the state of the system oscillates between two points. In contrast, the continuous-time model carves out a continuous trajectory (an example is shown in red).

The map between the canonical variables (p, u) and the tiling variables enables us to compute the Poisson brackets

$$8g\{X, Y\} = \frac{Y}{X} - 2XY - Y^2 + X^3Y + X^2Y^2. \quad (45)$$

These brackets look pretty complicated¹⁵ as they are quartic in X and Y . If we want to use tiling variables to describe the Hamiltonian dynamics of the string, then simpler brackets would strongly be preferable, especially since we eventually want to quantize the system. We thus consider another pair of coordinates defined by¹⁶

$$A := \frac{x_2}{y_2} = \frac{X}{Y}, \quad B := \frac{x_2}{y_1} = \frac{X}{X^{-1} - X - Y}.$$

¹⁵Quartic Poisson brackets also showed up in a related context in [54]. In contrast, the (quantum) integrable model of Goncharov and Kenyon [55] possessed much simpler quadratic Poisson brackets.

¹⁶These new coordinates can be defined for more complex segmented strings by taking ratios of x_i and y_i . They were labelled by p_i and q_i in [41, 47] and correspond to the faces of the tiling.

In the discrete model at the initial time or after an even number of time steps (32) gives

$$A_{\text{even}} = 2r_1^2 \geq 0, \quad B_{\text{even}} = 2r_2^2 \geq 0. \quad (46)$$

As far as tiling variables x_i, y_i with a fixed index i are concerned, each time step exchanges the role of the target space and the space of normal vectors. Namely, in Figure 4 a forward time step replaces $N_{12} \rightarrow R, Q \rightarrow N'_{23}$, etc., which changes the “meaning” of the cross-ratios of celestial variables. Accordingly, after an odd number of time steps we have a different expression in terms of the radii,

$$A_{\text{odd}} = -1 - 2r_1^2 - \frac{r_1^2}{r_2^2} < 0, \quad B_{\text{odd}} = -1 - 2r_2^2 - \frac{r_2^2}{r_1^2} < 0. \quad (47)$$

Although the signs change, we always have $\text{sgn } A = \text{sgn } B$ (assuming they are both non-zero). In the continuum model this continues to be true. In Figure 11, the boundaries separating positive and negative regions are indicated by thick black lines: the $X = 0$ and the $Y = 0$ lines separate positive and negative A regions, while B changes sign at the curved black lines. The Poisson brackets are rather simple,

$$4g\{A, B\} = A + B. \quad (48)$$

The Hamiltonian takes the form (cf. eqn. (16))

$$H(A, B) = 4g\sqrt{A + B + AB}.$$

We can further simplify the brackets by performing an additional change of coordinates,

$$\boxed{Z := \frac{B}{A + B}, \quad S := 4g(A + B).} \quad (49)$$

At this point, the interpretation of these new variables is somewhat obscure. We will see in section 6 that they provide an AdS generalization of the coordinates that appear in the 't Hooft equation. Eqns. (46) and (47) imply that the boundaries of the physically allowed region are

$$0 \leq Z \leq 1 \quad \text{and} \quad S \leq -\frac{4g}{Z(1-Z)} \quad \text{or} \quad S \geq 0, \quad (50)$$

which is displayed in Figure 11 (right). The two disjoint regions of the domain of S correspond to the two half-periods of oscillation ($\tilde{\rho} > 0$ and $\tilde{\rho} < 0$). It is interesting that the half-periods are treated asymmetrically in this coordinate system. The variables satisfy canonical brackets $\{S, Z\} = 1$, and the Hamiltonian is given by

$$H(S, Z) = \sqrt{4gS + Z(1-Z)S^2}. \quad (51)$$

Finally, from (44) we get the canonical transformation $(Z, S) \mapsto (p, u)$

$$\boxed{p = \log \frac{Z}{1-Z}, \quad u = 2g + SZ(1-Z).} \quad (52)$$

Second map

We can also start from the other off-diagonal component of the Lax matrix and consider $L_{21}(x) = 0$ along with the corresponding $L_{11}(x) = e^{-p}$. These equations give

$$X(p, u) = x^{-1} = \sqrt{\frac{u+2g}{u-2g}}, \quad Y(p, u) = -2g \frac{\tanh\left(\frac{p}{2}\right) + 1}{\sqrt{u^2 - 4g^2}} \operatorname{sgn} u. \quad (53)$$

These are the same formulas as (43), except that X and Y on the LHS have been transformed according to the discrete time evolution map (30). The inverse transformations are given by

$$u(X, Y) = -2g \frac{1+X^2}{1-X^2}, \quad p(X, Y) = -2 \tanh^{-1} \left(\frac{1-X^2-2XY}{1-X^2} \right), \quad (54)$$

which are the same as (44) with $u \mapsto -u$. The Poisson brackets of X and Y satisfy (45) if we multiply the RHS by -1 . In order to maintain (48), we flip the signs in the definitions of A and B ,

$$A := -\frac{x_2}{y_2} = -\frac{X}{Y}, \quad B := -\frac{x_2}{y_1} = -\frac{X}{X^{-1} - X - Y}.$$

Let us define Z and S as in (49),

$$Z := \frac{B}{A+B}, \quad S := 4g(A+B).$$

The boundaries of the physically allowed region are given by

$$0 \leq Z \leq 1 \quad \text{and} \quad S \leq 0 \quad \text{or} \quad S \geq \frac{4g}{Z(1-Z)}. \quad (55)$$

Z and S are still canonical variables and the Hamiltonian can be expressed as

$$H(S, Z) = \sqrt{-4gS + Z(1-Z)S^2}.$$

Finally, for the second map we obtain

$$\boxed{p = \log \frac{Z}{1-Z}, \quad u = -2g + SZ(1-Z)}. \quad (56)$$

This map is almost the same as (52) except for a $4g$ shift in u . Furthermore, note that the domain of S is also different in the two cases.

coordinates	description	Hamiltonian
$(\tilde{p}, \tilde{\rho})$	physical center-of-mass coordinates of the folded string (section 2)	$H_{\text{physical}} = \tilde{p} \cosh \tilde{\rho} + 4g \sinh \tilde{\rho} $
(p, u)	spectral curve coordinates (section 5.1)	$H_{\text{RS}} = 2 \cosh\left(\frac{p}{2}\right) \sqrt{u^2 - 4g^2}$
(Z, S)	canonical tiling variables: generalized momentum fraction and action variables	$H_{\text{ZS}} = \sqrt{\pm 4gS + Z(1-Z)S^2}$
(X, Y)	non-canonical tiling variables (section 4.2)	$H_{\text{XY}} = 4g \sqrt{\frac{X}{Y(1-X^2-XY)}}$
(A, B)	non-canonical “momentum” variables	$H_{\text{AB}} = 4g \sqrt{\pm A \pm B + AB}$

Table 1: Summary of various coordinates on the two-dimensional internal phase space of the four-segmented string in AdS₃ (or the folded string in AdS₂). In the expressions for the Hamiltonian, plus and minus signs correspond to the first and the second map, respectively.

Mixed map

So far we have found two distinct maps between the canonical variables (p, u) , which are associated to the spectral curve, and the (also canonical) tiling variables denoted by (Z, S) . The two maps can be transformed into one another by a shift

$$S \mapsto S \pm \frac{4g}{Z(1-Z)}.$$

The physical domain in either of the (Z, S) coordinate systems is somewhat awkward; see eqns. (50) and (55). Moreover, it is easy to show that in case of the first map we have the scaling,

$$S \propto \begin{cases} \frac{1}{g} & \text{for } u > 2g, \\ g & \text{for } u < -2g, \end{cases}$$

while the second map has the opposite behavior ($g \leftrightarrow g^{-1}$). As a consequence, taking the $g \rightarrow \infty$ flat space limit using either of these maps is cumbersome, because S scales differently in the two half-periods.

In section 6.2 we will see how a certain combination of these two maps appears in the lightcone quantization of a folded string. Namely, for $|u| \geq 2g$ (i.e. the physical region) we

define the following *mixed map*: for $u \geq 2g$ it is given by the first map, and for $u \leq -2g$ we switch to the second map. This drastically simplifies the boundaries of the physical region,

$$\boxed{0 \leq Z \leq 1 \quad \text{and} \quad S \in \mathbb{R}.}$$

In the two regions, $\text{sgn } S = \text{sgn } u$, and thus the Hamiltonian can be written as

$$\boxed{H(S, Z) = \sqrt{4g|S| + Z(1-Z)S^2}.} \tag{57}$$

This expression is one of the main results of the paper.

Taking the flat space limit is now simple. In both regions we have $S \propto g^{-1}$, which implies that $Z(1-Z)S^2$ in (57) is always subleading as $g \rightarrow \infty$. The Hamiltonian becomes $H_{\text{flat}} = \sqrt{4g|S|}$, which will also be computed in a more direct way in section 6.1.

6 Quantum spectral curve

6.1 The 't Hooft equation

The celebrated 't Hooft model [56] is an $SU(N_c)$ gauge theory in (1+1)-dimensions with Dirac fermions (quarks) in the fundamental representation. The theory is believed to share certain properties with QCD, such as quark confinement. 't Hooft solved the model in the lightcone gauge in the large- N_c limit where $\lambda \equiv g_{\text{YM}}^2 N_c$ is kept fixed [57]. Here g_{YM} denotes the coupling constant of the gauge theory. It turns out that free quarks are not present in the spectrum. Instead, it contains a tower of mesons, which are bound states of a quark and an antiquark. Meson wavefunctions are described by the 't Hooft equation,

$$\mu^2 \varphi(z) = \left[\frac{\alpha_1}{z} + \frac{\alpha_2}{1-z} \right] \varphi(z) - \int_0^1 dz' \frac{\varphi(z')}{(z' - z)^2}. \quad (58)$$

Here $z \in (0, 1)$ denotes the fraction of the total momentum carried by the quark, $\varphi(z)$ is the wavefunction and $\alpha_{1,2}$ are squares of renormalized quark masses. The dash on the integral sign indicates that the principal value must be taken. Assuming appropriate boundary conditions for the wavefunction, (58) is an eigenvalue equation for μ , which is the meson mass in units of $\sqrt{\lambda/\pi}$. The meson spectrum is discrete and exhibits a Regge-like behavior. Although exact solutions are not known in the general case, systematic analytic expansions do exist; see for instance [21]. For a simple numerical method for calculating the spectrum, we refer the reader to [58] where the integral equation has been recast into a matrix eigenvalue equation. (We will use the same technique to compute the spectrum of a modified 't Hooft equation in section 7.) For an extensive discussion of the 't Hooft model, we refer the reader to Coleman's lectures [59].

In the rest of the paper we will not be concerned with 2d $SU(N_c)$ gauge theory and the original derivation of the 't Hooft equation. We will take a different perspective and consider (58) as a Schrödinger equation, which quantizes the folded string in flat space (see Figure 1). The derivation goes as follows. One writes the two-body Hamiltonian for the string with two endpoints

$$H_2 = (p_1^2 + m_1^2)^{\frac{1}{2}} + (p_2^2 + m_2^2)^{\frac{1}{2}} + \kappa |x_1 - x_2|.$$

The coordinates are canonical, i.e. $\{x_i, p_j\} = \delta_{ij}$ and all the other brackets vanish. Later on we will set $\kappa = \frac{L^2}{\pi\alpha'} = 2g$ to make contact with the units we used in section 2. Quantizing in these coordinates is problematic, because one cannot restrict the relativistic system to the truncated two-particle Fock-space while preserving Lorentz invariance [60–62].

Let us try to evade the anomaly by switching to a different coordinate system. Following [61–64], we separate center-of-mass and relative motion by considering the canonical

transformation,

$$x_{1,2} = x_0 \pm \frac{x'}{2}, \quad p_{1,2} = \frac{p_0}{2} \pm p', \quad (59)$$

and go to the infinite momentum frame by taking the $p_0 \rightarrow \infty$ limit. We can write the square of the invariant mass as

$$M^2 = H_2^2 - p_0^2 \approx 2p_0(H_2 - p_0) = \frac{m_1^2}{z} + \frac{m_2^2}{1-z} + 2\kappa|s|, \quad (60)$$

where we defined the momentum fraction variable z and the conjugate (signed) action variable s ,

$$z := \frac{p_1}{p_1 + p_2}, \quad s := x'(p_1 + p_2), \quad (61)$$

which satisfy $\{s, z\} = 1$. Let us now promote (60) to a Schrödinger equation,

$$M^2\varphi(z) = \left[\frac{m_1^2}{z} + \frac{m_2^2}{1-z} + 2\kappa|s| \right] \varphi(z). \quad (62)$$

The action of $|s|$ can be found by Fourier transforming the wavefunction, multiplying it by $|s|$, and then Fourier transforming back into z -space,

$$|s|\varphi(z) = \lim_{\epsilon \rightarrow 0} \frac{1}{\pi} \int_{-\infty}^{\infty} dz' \int_0^{\infty} ds s \cos[s(z' - z)] e^{-\epsilon s} \varphi(z') = -\frac{1}{\pi} \int_{-\infty}^{\infty} dz' \frac{\varphi(z')}{(z' - z)^2}.$$

In order to remove negative energy states, we project on non-negative momenta. The conditions $p_{1,2} \geq 0$ require $z \geq 0$ and $z \leq 1$, respectively. This restricts the integration domain and thus the Schrödinger equation becomes the 't Hooft equation (62) with the identification $\mu^2 = \frac{\pi M^2}{4g}$.

6.2 Canonical variables in flat space

The spectral curve of the folded string in AdS_3 space is given in (38), which we copy here for convenience,

$$e^p + e^{-p} + 2 - \frac{M^2}{u^2 - 4g^2} = 0.$$

Here p and u are canonically conjugate variables. The classical configuration space consists of the union of two half-lines $|u| \geq 2g$. At $u = \pm 2g$, the two particles collide. The flat space limit is achieved by sending $g \rightarrow \infty$ while keeping the string energy fixed.

Assuming u is real, we can define a new coordinate

$$q := \begin{cases} u - 2g & \text{for } u \geq +2g, \\ u + 2g & \text{for } u \leq -2g. \end{cases} \quad (63)$$

coordinates	description	Hamiltonian
$(\tilde{p}, \tilde{\rho})$	physical momentum and position (section 2)	$H_{\text{physical}} = \tilde{p} + 4g \tilde{\rho} $
(p, q)	spectral curve coordinates in the $g \rightarrow \infty$ limit	$H_{\text{RS}} = 4 \cosh\left(\frac{p}{2}\right) \sqrt{g q }$
(z, s)	parton momentum fraction and action variable	$H_{\text{null}} = \sqrt{4g s }$

Table 2: Canonical coordinates for the folded string in flat space.

This effectively cuts out the $u \in (-2g, 2g)$ region, which is not part of the classical configuration space. Let us rescale the energy,

$$\mu^2 := \frac{\pi M^2}{4g} .$$

Taking the $g \rightarrow \infty$ limit while keeping μ fixed gives a non-analytic equation, the (real) spectral curve

$$e^p + e^{-p} + 2 - \frac{\mu^2}{\pi|q|} = 0 . \quad (64)$$

In the following, we work out the canonical transformations between flat space variables. The discussion is parallel to section 5.4, where we introduced the relevant tiling variables in the case of AdS target space. Although some of the maps are going to be straightforward limits of their AdS counterparts, they can also be obtained by simple trial and error, because as Figure 12 shows, the time evolution of the variables is rather simple. A summary of the relevant canonical variables that we are using is presented in Table 2. Our goal is to determine a direct map between the variables (z, s) , which we used in lightcone quantization, and (p, q) , the spectral curve coordinates. This will allow us to convert the 't Hooft equation, which is written in the z -basis, into a difference equation in the q -basis.

The relationship between $(\tilde{p}, \tilde{\rho})$ and (p, q) can be determined from (41) by taking the $g \rightarrow \infty$ limit and examining the four possibilities (depending on the signs of p and q) on a case-by-case basis. We get

$$p = (\text{sgn } \tilde{p}) \log \left(1 + \frac{|\tilde{p}|}{2g|\tilde{\rho}|} \right) , \quad q = \frac{1}{2} \tilde{\rho} (|\tilde{p}| + 2g|\tilde{\rho}|) , \quad (65)$$

which is a canonical transformation if $\tilde{\rho} \neq 0$ and $\tilde{p} \neq 0$. The Hamiltonian (40) simplifies to

$$H_{\text{RS}}(p, q) = 4 \cosh\left(\frac{p}{2}\right) \sqrt{g|q|} .$$

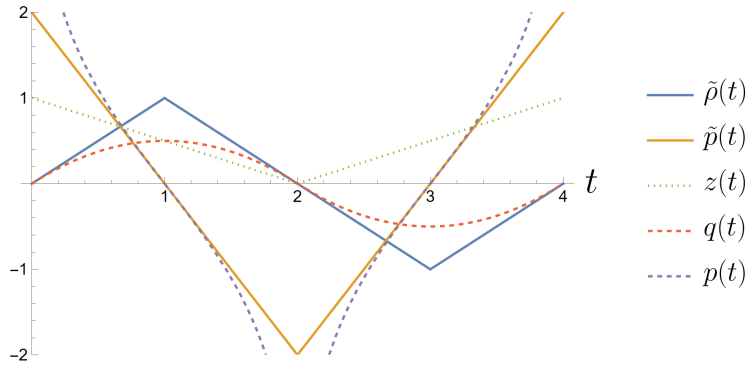


Figure 12: Time evolution of dynamical variables of the folded string in flat space ($g = \frac{1}{2}$). Here $\tilde{\rho}$ is the physical position of one of the particles at the end of the string (see Figure 1), \tilde{p} is the conjugate momentum, z is the momentum fraction variable from eqn. (61), and p and q denote (non-analytic) spectral curve coordinates; see eqn. (63).

The solution $q(t)$ consists of parabolas glued together as shown in Figure 12 (red dashed curve). Setting $m_1 = m_2 = 0$ in eqn. (60) allows us to express s in terms of $(\tilde{p}, \tilde{\rho})$

$$s = \frac{H^2}{4g} \text{sgn } \tilde{\rho} = \frac{\text{sgn } \tilde{\rho}}{4g} (|\tilde{p}| + 4g|\tilde{\rho}|)^2. \quad (66)$$

The expression includes an extra factor of $\text{sgn } \tilde{\rho}$. This is necessary, otherwise the map $(\tilde{p}, \tilde{\rho}) \mapsto (z, y)$ would be two-to-one.

Note that s is frozen due to the infinite boost and it changes discontinuously whenever $\tilde{\rho}$ changes sign, i.e. when the quarks collide. Its time evolution is given by the Poisson bracket

$$\dot{s} = \{s, H\} = \frac{\tilde{p}^2}{4g} \frac{d}{d\tilde{\rho}} \text{sgn } \tilde{\rho} = |s| \frac{d}{d\tilde{\rho}} \text{sgn } \tilde{\rho},$$

which is consistent with the jump. In contrast, z changes continuously between 0 and 1, and we can determine its expression by demanding $\{\tilde{\rho}, \tilde{p}\} = 1$ and $\{s, z\} = 1$. We get

$$z = \frac{\vartheta(\tilde{p})\tilde{p} + 2g|\tilde{\rho}|}{|\tilde{p}| + 4g|\tilde{\rho}|}, \quad (67)$$

where $\vartheta(x)$ is the Heaviside step function. This map is a special case of the map obtained in [65]. The Hamiltonian $H = M$ is independent of z ,

$$H_{\text{null}}(z, y) = \sqrt{4g|s|}. \quad (68)$$

Note that the constant g can be eliminated from the maps by rescaling $\tilde{\rho} \rightarrow \tilde{\rho}/\sqrt{g}$ and $\tilde{p} \rightarrow \tilde{p}\sqrt{g}$. Inverting the formulas (66) and (67) gives

$$\tilde{p} = 2(2z - 1)\sqrt{g|s|}, \quad \tilde{\rho} = \frac{1}{\sqrt{g}} [\vartheta(2z - 1) - z \operatorname{sgn}(2z - 1)] \sqrt{|s|} \operatorname{sgn} s. \quad (69)$$

This result finally allows us to relate the coordinate pairs $(z, s) \mapsto (\tilde{p}, \tilde{\rho}) \mapsto (p, q)$. Using (65) and (69) we get the simple relationship

$$\boxed{p = \log \frac{z}{1-z}, \quad q = sz(1-z)}. \quad (70)$$

The map is a canonical transformation between $0 < z < 1$ and singular at the boundaries of the interval where p diverges. Note that the first expression, along with the definition $z \equiv \frac{p_1}{p_1 + p_2}$, implies that p can be interpreted as the rapidity difference between the quark and antiquark, i.e. the quark momenta can be written as $p_{1,2} = \bar{p}e^{\pm \frac{p}{2}}$.

6.3 Quantum spectral curve in flat space

In this section, we will recall how the 't Hooft equation can be converted into a finite difference equation [21]. Since the folds of the yoyoing string in Figure 1 move with the speed of light, we will henceforth set the renormalized quark masses in (58) to zero. Hence, our starting point is the equation,

$$\mu^2 \varphi(z) = - \int_0^1 dz' \frac{\varphi(z')}{(z' - z)^2}, \quad (71)$$

which we would like to relate to the classical spectral curve of the folded string.

Boundary layer equation

In order to calculate the wavefunctions by a matched asymptotic expansion, the authors of [58] considered the boundary layer near $z = 0$. By means of a Fourier transformation, they derived a difference equation from (71), which we will now review as a warm-up exercise. Let us define the boundary layer variable $\xi = z\mu^2$. This eliminates μ from the equation,

$$\varphi(\xi) = - \int_0^\infty d\eta \frac{\varphi(\eta)}{(\eta - \xi)^2}.$$

After changing to rapidity coordinates $\xi = e^\theta$, the 't Hooft equation becomes

$$\varphi(\theta) = - \frac{e^{-\theta}}{4} \int_{-\infty}^\infty d\theta' \frac{\varphi(\theta')}{\sinh^2\left(\frac{\theta - \theta'}{2}\right)}.$$

After multiplying both sides by e^θ and performing a Fourier transformation¹⁷

$$\chi(\nu) = \frac{1}{\sqrt{2\pi}} \int_{-\infty}^{\infty} d\theta e^{i\nu\theta} \varphi(\theta),$$

we get

$$\chi(\nu - i) = \pi\nu \coth(\pi\nu) \chi(\nu). \quad (72)$$

The equation can be solved in terms of the Barnes G-function [21].

Quantum spectral curve

Following [21], we can also convert (71) into a finite difference equation without restricting our attention to a boundary layer. Let us first switch to spectral curve momentum coordinates $z \rightarrow p$ via the transformation that we have found in (70). This change of variables has also been used in [66]. The 't Hooft equation becomes

$$\mu^2 \varphi(p) = -\cosh^2\left(\frac{p}{2}\right) \int_{-\infty}^{\infty} dp' \frac{\varphi(p')}{\sinh^2\left(\frac{p-p'}{2}\right)}.$$

After dividing by $4\cosh^2\left(\frac{p}{2}\right)$ and Fourier transforming $\varphi(p) \rightarrow \psi(\nu)$, we get

$$\frac{\mu^2}{2\pi} \int_{-\infty}^{\infty} d\nu' S(\nu - \nu') \psi(\nu') = \pi\nu \coth(\pi\nu) \psi(\nu),$$

where the kernel S is given by

$$S(\nu) = \frac{\pi\nu}{\sinh(\pi\nu)}.$$

Let us define the Q -function [21]

$$Q(\nu) := \nu \cosh(\pi\nu) \psi(\nu). \quad (73)$$

Then for the strip $-1 < \text{Im } \nu < 1$ we have

$$Q(\nu) = \frac{\mu^2}{2\pi} \sinh(\pi\nu) \int_{-\infty}^{\infty} d\nu' \frac{\nu - \nu'}{\nu'} \cdot \frac{1}{\cosh \pi\nu'} \cdot \frac{1}{\sinh \pi(\nu - \nu')} Q(\nu').$$

If we shift the argument, then according to the Sokhotski–Plemelj theorem (appropriately modified for the strip; see e.g. [6] for a similar calculation), we get an extra term on the boundary

$$Q(\nu \pm i) = -\frac{\mu^2 \tanh(\pi\nu)}{2\pi \nu} Q(\nu) + \frac{\mu^2}{2\pi} \sinh(\pi\nu) \int_{-\infty}^{\infty} d\nu' \frac{\nu \pm i - \nu'}{\nu'} \cdot \frac{1}{\cosh \pi\nu'} \cdot \frac{1}{\sinh \pi(\nu - \nu')} Q(\nu').$$

¹⁷Note that a Fourier transformation in rapidity coordinates is equivalent to a Mellin transformation.

Using these expressions one can show that $Q(\nu)$ satisfies the following difference equation,¹⁸

$$\boxed{Q(\nu + i) + Q(\nu - i) - 2Q(\nu) = -\mu^2 \frac{\tanh(\pi\nu)}{\pi\nu} Q(\nu)}. \quad (74)$$

This equation¹⁹ was first derived in [21]. The authors have developed an analytic method to determine the meson mass spectrum using a systematic expansion. For further details, we refer the reader to [21].

Our claim is that it can be interpreted as the quantized spectral curve of the folded string in Figure 1. The classical spectral curve of the string is given in (64), which we copy here for convenience,

$$e^p + e^{-p} + 2 - \frac{\mu^2}{\pi|q|} = 0. \quad (75)$$

After identifying $\nu = q$, the relationship of (74) and (75) are clear. Let us assume that the state is described by a wavefunction $\psi(q)$, which vanishes if we act on it by an (appropriately defined) operator version of (75). Taking the representation $\hat{p} = -i\partial_q$ and $\hat{q} = q$, the exponential of the momentum becomes a shift operator

$$e^{\pm p}\psi(q) = \psi(q \pm i).$$

In the classical (large ν) limit, we have $\tanh(\pi\nu) \rightarrow \text{sgn } \nu$, and (74) reduces to (75) modulo a minus sign multiplying $e^p + e^{-p}$. This is due to the definition of Q in (73), which contained the factor $\cosh(\pi\nu)$, an antiperiodic function under the shift $\nu \rightarrow \nu + i$. We emphasize that at this point it is unclear how to directly quantize (75) and why we must replace $|q| \mapsto q \coth \pi q$. We leave this for future work.

6.4 Quantum spectral curve in AdS

The results of the previous section can be extended to AdS by noticing that in the $g \rightarrow \infty$ limit we can relate flat space coordinates to tiling variables in AdS,

$$(A, B) = \frac{x'}{4g}(p_1, p_2),$$

where x' is the relative position and p_1, p_2 are the particle momenta from (59). In fact, with the above identification the Poisson bracket (48) follows from $\{x_i, p_j\} = \delta_{ij}$ even away from $g = \infty$. Furthermore, we have

$$(Z, S) = (z, s).$$

¹⁸Note that the boundary layer difference equation (72) can be recovered from (74) by plugging in $Q(\nu) = \nu(-\mu^2)^{-i\nu}\chi(\nu)$ and then taking the large μ^2 limit.

¹⁹Note the factor of two difference between the definition of ν in [21] and our notation.

Moreover, the coordinate transformation (70), which is valid in flat space, is consistent with its AdS counterpart given in (52) and (56) for the two maps. Finally, the Hamiltonian (68) is the flat space limit of (57). Having identified the tiling variables and the Hamiltonian as a one-parameter deformation of the flat space system, we can now promote them to operators.

The case of $g = 0$

This case is simple, because the first and second maps coincide and we do not need to take absolute values. First, setting $g = 0$ in the classical spectral curve (38) gives

$$e^p + e^{-p} + 2 - \frac{M^2}{u^2} = 0. \quad (76)$$

On the other hand, by taking the square of (57) we obtain

$$M^2\varphi(z) = \hat{S}\hat{Z}(1 - \hat{Z})\hat{S}\varphi(z), \quad (77)$$

where we have symmetrized the operator on the RHS, which acts on the wavefunction $\varphi(z)$ where $z \in [0, 1]$. Taking the representation $\hat{Z} = z \cdot$ and $\hat{S} = -i\partial_z$, we obtain

$$z(1 - z)\varphi''(z) + (1 - 2z)\varphi'(z) + M^2\varphi(z) = 0. \quad (78)$$

The term on the RHS of (77) has been proposed as an effective confining potential to capture the nonperturbative dynamics in hadron physics [67]. Eqn. (78) has been analyzed in [68] in the context of the XXX Heisenberg spin chain for zero spin and two sites. The corresponding Baxter equation in [68] is nothing but the quantized classical curve (76).

Note that in terms of the momentum variable $p = \log \frac{z}{1-z}$ the equation is cast into a scattering equation with the Pöschl–Teller potential,

$$\varphi''(p) + \frac{M^2}{4 \cosh^2\left(\frac{p}{2}\right)}\varphi(p) = 0,$$

and it is well-known that the potential is reflectionless precisely if

$$M^2 = n(n + 1), \quad n = 0, 1, 2, \dots \quad (79)$$

This formula also gives the spectrum. Notice that the calculation does not require anything extraordinary, since in the $g = 0$ case, the physical domain of u is the entire real line; therefore no issues arise regarding the definition of the p -basis.

Note that we could have symmetrized the operator $Z(1 - Z)S^2$ in the opposite way. The relationship between the two ordering is given by

$$[\hat{Z}(1 - \hat{Z})]^{\frac{1}{2}}\hat{S}^2[\hat{Z}(1 - \hat{Z})]^{\frac{1}{2}}\varphi(z) - \hat{S}\hat{Z}(1 - \hat{Z})\hat{S}\varphi(z) = \frac{1}{4} \left[\frac{1}{z} + \frac{1}{1 - z} \right] \varphi(z),$$

which is proportional to the mass term in the 't Hooft equation (58). If we multiply the RHS by m^2 and add it to the RHS of (77), then the equation can still be solved analytically in terms of Jacobi polynomials [67]. The corresponding eigenvalues are

$$M^2 = (n + |m|)(n + |m| + 1), \quad n = 0, 1, 2, \dots$$

Finite g spectral curve

At finite g values, the 't Hooft equation acquires another term (again we change $Z \rightarrow z$),

$$\mu^2 \varphi(z) = - \int_0^1 dz' \frac{\varphi(z')}{(z' - z)^2} - \frac{\pi}{4g} [z(1 - z)\varphi''(z) + (1 - 2z)\varphi'(z)]. \quad (80)$$

After switching to the p coordinate we have

$$\mu^2 \varphi(p) = - \cosh^2 \left(\frac{p}{2} \right) \int_{-\infty}^{\infty} dp' \frac{\varphi(p')}{\sinh^2 \left(\frac{p-p'}{2} \right)} - \frac{\pi}{g} \cosh^2 \left(\frac{p}{2} \right) \varphi''(p). \quad (81)$$

Similarly to the previous section we now perform a Fourier transformation and switch to the Q -function defined by,

$$Q(\nu) := \left[\nu \cosh(\pi\nu) + \frac{\nu^2}{4g} \sinh(\pi\nu) \right] \psi(\nu).$$

By naively repeating the same steps as before we get the difference equation,

$$Q(\nu + i) + Q(\nu - i) - 2Q(\nu) = - \frac{\mu^2}{\frac{\pi\nu^2}{4g} + \pi\nu \coth(\pi\nu)} Q(\nu). \quad (82)$$

This is to be compared with the classical spectral curve (38) in the q coordinate defined by (63). In this case we do not take the large- g limit so that we obtain the following non-analytic spectral curve,

$$e^p + e^{-p} + 2 - \frac{\mu^2}{\frac{\pi q^2}{4g} + \pi|q|} = 0. \quad (83)$$

Indeed, by comparing (82) and (83) we see that the difference equation can be interpreted as the quantum spectral curve.

It should be mentioned that eqns. (74) and (82) are different from the quantum spectral curves that appear in the literature in a crucial aspect, namely that their classical limit is not analytic. The reason for this is that the classical phase space of the folded string in the (z, s) coordinates is mapped to the spectral curve coordinates (p, u) via the ‘‘mixed map’’ of section 5.4, which contained absolute values and was only defined for $u \in \mathbb{R}$.

7 Numerical spectrum

In this section we will numerically solve the modified 't Hooft equation (80), which governs the wavefunction of the internal degree of freedom of the four-segmented string in AdS₃ (or that of the folded string in AdS₂). The equation is an eigenvalue equation for μ and it contains a single parameter g , which sets the size of AdS. The spectrum is already known in two different limits. As $g \rightarrow \infty$, we recover the 't Hooft equation, which has been studied extensively starting with [56,58,69]. On the other hand, by plugging in $\mu^2 \rightarrow \frac{\pi M^2}{4g}$ and taking $g = 0$ one obtains (78) and the spectrum should match the result in eqn. (79). Following [58], let us define a new coordinate θ by setting $z = \frac{1}{2}(1 - \cos \theta)$ and expand the wavefunction

$$\varphi(z) = \sum_{k=1}^{\infty} a_k \sin k\theta.$$

By plugging this into the modified 't Hooft equation (80), multiplying by $\frac{2}{\pi} \sin l\theta$ and integrating w.r.t. θ , we arrive at a matrix eigenvalue problem,

$$\mu^2 a_k = (V + \frac{\pi}{4g} U)_{kl} a_l$$

where for the elements of V and U we obtain

$$V_{kl} = -\frac{4}{\pi} \int_0^\pi d\theta \sin k\theta \int_0^\pi d\theta' \frac{\sin \theta' \sin l\theta'}{(\cos \theta - \cos \theta')^2} = 4l \int_0^\pi d\theta \frac{\sin k\theta \sin l\theta}{\sin \theta},$$

$$U_{kl} = \frac{2l}{\pi} \int_0^\pi d\theta [l \sin l\theta - \cos l\theta \cot \theta] \sin k\theta.$$

The integrals can be evaluated explicitly; see e.g. Appendix A in [70]. For the first column of V we get,

$$V_{k,1} = \begin{cases} \frac{8}{k} & \text{for } k = \text{odd}, \\ 0 & \text{for } k = \text{even}. \end{cases}$$

For $l > 1$ we have,

$$V_{kl} = \begin{cases} 0 & \text{for } k+l = \text{odd}, \\ \frac{8l}{k+l-1} + \frac{l}{l-1} V_{k-1,l-1} & \text{for } k+l = \text{even}, \end{cases}$$

where $V_{0,l} = V_{k,0} = 0$. In order to compute U_{kl} notice that whenever the integral does not trivially vanish due to the symmetries of the integrand, then $\cos l\theta \cot \theta \sin k\theta$ can be written as a $\sum_n c_n \cos(2n\theta)$ and only the constant term $c_0 = 0, \frac{1}{2}$ or 1 contributes to the integral. We obtain,

$$U_{kl} = \begin{cases} 0 & \text{for } k < l \text{ or } k+l = \text{odd}, \\ k(k-1) & \text{for } k = l, \\ -2l & \text{otherwise.} \end{cases}$$

n	μ_n^2/π^2	n	μ_n^2/π^2
1	0.737061746	6	5.75049262
2	1.753731337	7	6.74962942
3	2.748160912	8	7.75028440
4	3.751057582	9	8.74977158
5	4.749295381	10	9.75018514

Table 3: The first ten eigenvalues at $g = \infty$ computed using 500×500 matrices. The computation time on a laptop was about one minute. The results are in agreement with the literature; see for instance [21].

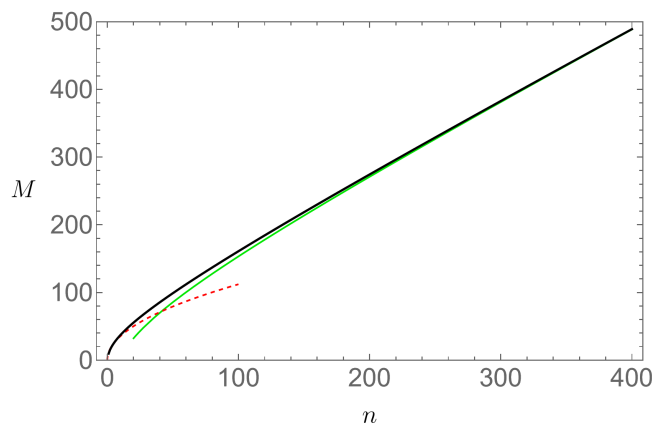


Figure 13: The first 400 eigenvalues at $g = 10$. Green line indicates the semiclassical result $M = n + \frac{8g}{\pi} \log n + \text{const.}$ from eqn. (7). Red dashed line shows the Regge trajectory (6).

Note that the U and V matrices are not Hermitean, because we used a basis which is orthogonal with a different inner product. Nevertheless, the sum $V + \frac{\pi}{4g}U$ has real and positive eigenvalues when $g \geq 0$. In our basis, U is an upper triangular matrix, whose eigenvalues equal the values in the diagonal, thereby confirming the $g = 0$ result (79).

For practical numerical calculations we will truncate the matrices. With a size of 500×500 , one is able to obtain several significant digits, and the calculations typically only take a few minutes on a laptop. The first ten (squared) energy eigenvalues at $g = \infty$ are given in Table 3. This result is well known in the literature.

Figure 13 shows the eigenvalues at $g = 10$ where the modifying term in (80) (which is proportional to $1/g$) starts playing a role. With decreasing g , the spectrum becomes more and more linear and approaches the $g = 0$ result (79).

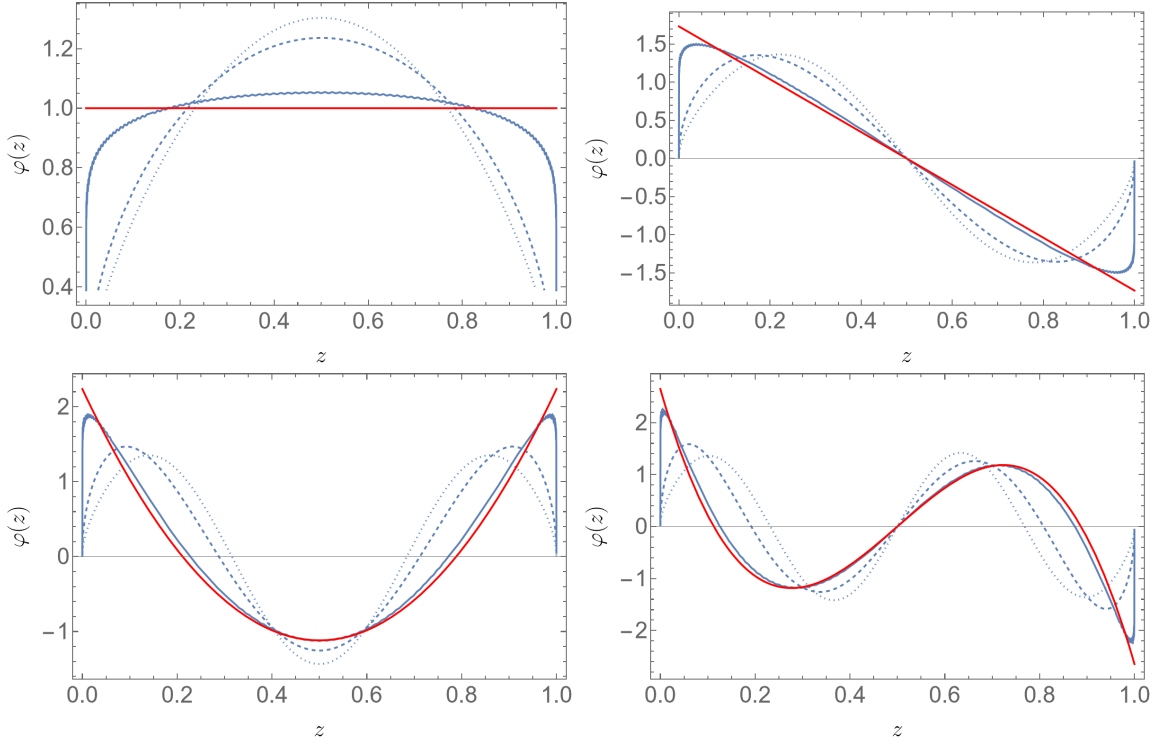


Figure 14: The first four eigenfunctions $\varphi^{(n)}(z)$ at $g = \frac{1}{100}$ (solid line), $g = \frac{1}{2}$ (dashed line), and $g = 100$ (dotted line). Red curves show the analytical result at $g = 0$.

Figure 14 shows the wavefunctions of the four lowest lying states at various values of g . The analytical form of the wavefunction is only known at $g = 0$, in which case it can be expressed in terms of Legendre polynomials. Equation (80) is symmetric under the exchange $z \mapsto 1 - z$ and thus the wavefunctions are either symmetric or antisymmetric. The only qualitative difference between $g = 0$ and $g > 0$ is the behavior of the wavefunctions near $z = 0, 1$. These points correspond to the quark collision events (i.e. $\tilde{\rho} = 0$ in Figure 1).

Finally, Figure 15 shows the first ten energy eigenvalues as a function of g . At $g = \infty$, eqn. (80) reduces to the 't Hooft equation, whose spectrum lies on a nearly linear Regge trajectory. The plot interpolates between this spectrum and the $M_n^2 = n(n + 1)$ result at $g = 0$. Since $g \propto L^2$, from the perspective of the four-segmented string changing g is tantamount to changing the AdS radius. Note that the $g = 0$ case is the highly quantum tensionless limit ($\alpha' \rightarrow \infty$). Interestingly, the spectrum seems to be compatible with expectations based on a hypothetical free holographic dual theory with evenly spaced operator dimensions.

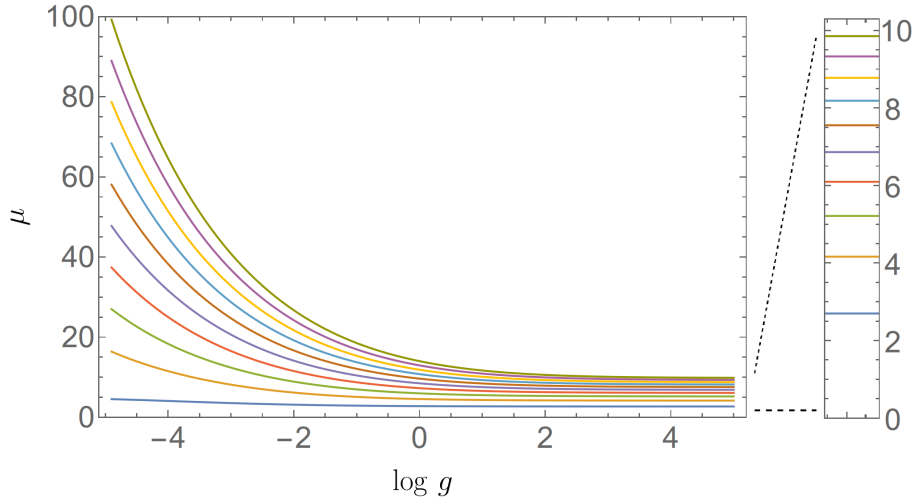


Figure 15: The first ten energy eigenvalues of the modified 't Hooft equation plotted as a function of $g = \frac{L^2}{2\pi\alpha'}$ (here L is the AdS radius). The spectrum interpolates between approximately equal spacing at low g and Regge behavior at large g .

8 Discussion

In this paper, we attempted to establish a link between lightcone quantization and quantum spectral curves. In order to clarify their relationship, we considered the simple system of a folded string, which is depicted in Figure 1. The one-directional motion of the string is oscillatory and the endpoints always move with the speed of light. In flat space, the system is amenable to lightcone quantization, which uses an infinitely boosted frame and a projection on non-negative particle momenta, thereby avoiding a Poincaré anomaly in the quantum theory [62]. The center-of-mass coordinates decouple and canonical quantization of the fractional momentum and conjugate action variables lead to the 't Hooft equation.

From a certain perspective, the folded string is a degenerate system, because it contains both particles and string segments. Furthermore, having a flat target space is slightly more complicated from a spectral curve point of view. For this reason, we generalized the setup and considered a four-segmented string in AdS_3 (see Figure 3), which in a squashed limit reduces to the folded string. We investigated its phase space and computed its classical spectral curve by means of planar bipartite graphs (a.k.a. brane tilings or on-shell diagrams). As it turns out, the phase space of the internal degree of freedom of the four-segmented string in AdS_3 is identical to that of the folded string in AdS_2 . We found a canonical pair of “separated” variables on the spectral curve, denoted by (p, u) . Physical positions of the particles at the end of the folded string can be obtained from certain level sets, which is familiar from the

way one computes soliton positions in 2d relativistic integrable theories from the associated Ruijsenaars-Schneider model.

Using the Baker-Akhiezer function, we managed to map (p, u) onto the natural tiling variables (Z, S) in two different ways, dubbed the *first map* and the *second map*. These are asymmetric maps, which correspond to the two half periods of the oscillation. The correct map to the variables that appear in the 't Hooft equation turned out to be a certain combination of the two maps, termed the *mixed map*.

These maps between phase spaces allowed us to identify the integral transformed 't Hooft equation (74) (first calculated in [21]) as the quantum spectral curve of the folded string. Moreover, our findings suggested a natural generalization of the results to four-segmented strings in AdS₃. In AdS, the 't Hooft equation is modified by an extra term,

$$\mu^2 \varphi(z) = - \int_0^1 dz' \frac{\varphi(z')}{(z' - z)^2} + \frac{\pi}{4g} (-i\partial_z) z(1 - z) (-i\partial_z) \varphi(z), \quad (84)$$

where g is the square radius of AdS in units of $2\pi\alpha'$. In the context of hadron physics, this term has previously been proposed as an effective confining potential to capture the non-perturbative dynamics of QCD [67]. Here it arises as a contribution from the curvature of the AdS target space. It is remarkable that this simple additive term captures all the differences between flat space and AdS. We have solved the equation numerically for various values of g and showed that the spectra interpolate between $\mu^2 = \frac{\pi}{4g} n(n + 1)$ in the $g \rightarrow 0$ limit and 't Hooft's nearly linear Regge trajectory as $g \rightarrow \infty$. The $g \rightarrow 0$ limit of (84) has been analyzed in [68] in the context of a two-site spin chain with zero spins. It would be interesting to understand the folded string from a spin chain perspective.

A few comments regarding the quantum spectral curve are in order. We have derived the difference equation (74) by a transformation applied to the 't Hooft equation and at this point it is unclear how to obtain it by a direct quantization of the classical curve (64). A peculiar feature of the quantum spectral curve is that its classical counterpart is non-analytic. The non-analyticity arises from the fact that the lightcone coordinates and the spectral curve coordinates are related by the mixed map, which switches between the two canonical maps depending on the sign of u .

We note that it seems possible to quantize the folded string using either the first or the second map instead of the mixed map. The situation is complicated by the fact that the naive representation $\hat{S} = -i\partial_z$ is not self-adjoint on the $z \in [0, 1]$ interval and thus this approach requires extra care. The corresponding quantum spectral curve would presumably resemble more closely those in the literature as the classical limit would be an ordinary analytic spectral curve. This will be investigated elsewhere.

Several other research directions would be interesting to pursue. We list a few of them here:

- One might try to directly quantize the $\mathfrak{sl}(2)$ Ruijsenaars-Schneider Hamiltonian (40). This presumably involves some sort of symmetrization prescription.
- It would be useful to find the correct Dirac brackets for celestial variables. This would allow one to study the quantum algebra of the generators of the $SO(2, n)$ symmetry group of AdS and decide if an anomaly appears or not.
- It would be interesting to prove the conjecture in the Appendix about the equivalence of the closing constraints and the vanishing of the adjugate Kasteleyn matrix at two special points for strings of an arbitrary number of segments.
- Segmented strings can also be defined in essentially the same way on de Sitter or BTZ backgrounds [35]. It would be interesting to extend our results to these spacetimes.
- In this paper we studied the simplest closed string, which had only one internal degree of freedom. It would be interesting to understand how the results generalize to strings with more than four segments.

We hope to address some of these questions in the future.

Acknowledgments

I am grateful to Paolo Benincasa, Berzel Boldis, Andrea Cavaglià, Sergei Dubovsky, Sebastián Franco, Alba Grassi, Cristoforo Iossa, Péter Lévy, Vladimir Rosenhaus, Torben Skrzypek, Bogdan Stefanski, Alessandro Torrielli and Congkao Wen for interesting discussions and Torben Skrzypek and Alessandro Torrielli for valuable comments on the draft. I thank Jeffrey Forshaw and Ruben Sandapen for pointing out an error in an earlier version of the manuscript. I thank the CUNY Graduate Center and New York University for hospitality. I gratefully acknowledge discussions with the participants of the “CFT and Holography” meeting at Trinity College Dublin and at the “Integrability in Gauge and String Theory 2022” conference at Eötvös University in Budapest where some of the results were first presented. The author has been supported by the STFC Ernest Rutherford grant ST/P004334/1.

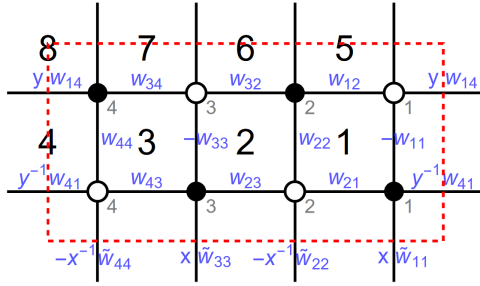


Figure 16: Weights associated to edges in the tiling.

A Closing constraints and the adjugate Kasteleyn matrix

In this Appendix, we relate the closing constraints (28) to properties of the so-called Kasteleyn matrix of the tiling. The Kasteleyn matrix is the dressed adjacency matrix of the graph. Its rows and columns are labelled by the black and white nodes of the tiling and thus in the case of a four-segmented string, it is a 4×4 matrix. Two special parameters, x and y , multiply those edges that cross the boundaries of the fundamental domain (red dashed lines in Figure 16). Depending on the orientation of the tiling edge (i.e. on which side of the boundary the black node lies) we multiply the weights by x or x^{-1} and y or y^{-1} (or possibly a combination for more complicated tilings). Finally, minus signs also have to be distributed on the edges, such that their product around a face F is given by,

$$\prod_{i \in \{\text{edges around } F\}} s_i = \begin{cases} +1 & \text{if } e_F = 2 \pmod{4} \\ -1 & \text{if } e_F = 0 \pmod{4} \end{cases}, \quad (85)$$

where e_F denotes the number of edges around F . Such an assignment of minus signs is always possible. For a detailed discussion, we refer the reader to [41].

Let us now focus on the square tiling that is relevant for the four-segmented string and assign 16 unfixed weights to its edges as in Figure 16. The Kasteleyn matrix is easy to compute,

$$K = \begin{pmatrix} x\tilde{w}_{11} - w_{11} & w_{12} & 0 & yw_{14} \\ w_{21} & w_{22} - x^{-1}\tilde{w}_{22} & w_{23} & 0 \\ 0 & w_{32} & x\tilde{w}_{33} - w_{33} & w_{34} \\ y^{-1}w_{41} & 0 & w_{43} & w_{44} - x^{-1}\tilde{w}_{44} \end{pmatrix}.$$

For each function on the nodes, one can associate a gauge transformation on the edge weights in the following way. At a white (black) node the transformation multiplies (divides) the weights of all edges incident to that node by the function value. Edge weights related by gauge transformations are equivalent. Note that constant functions give trivial gauge transformations, because each edge weight is divided and multiplied by the same number. In the four-segmented case, there are 16 tiling edges, 8 nodes and therefore a 7d space of gauge transformations. This leaves us with $16 - 7 = 9$ independent variables before demanding that the closing constraints are satisfied.

Note that in a certain gauge the edge weights are simply given by the x_i, y_i variables, which in this gauge appear on the edges according to Figure 6 (left). The spectral curve can also be computed using the Kasteleyn matrix by taking the determinant,

$$\det K(x, y) = 0,$$

which gives the same result as before in (20) and (34).

Although we already have the expression (28) for the closing constraints, we will now make an observation, which transforms the constraints into a form that is more natural in the language of the tiling and could perhaps generalize to other cases. For this we will need the definition of the adjugate of the Kasteleyn matrix,

$$\text{adj } K := K^{-1} \det K.$$

The observation is that the constraints are equivalent to demanding that the adjugate matrix vanishes at two special points

$$\boxed{\text{adj } K = 0, \quad \text{at } x = \pm 1, \ y = -1.} \tag{86}$$

A lengthy, but straightforward calculation shows that demanding (86) gives precisely seven constraints on the edge weights, which finally gives a $9 - 7 = 2$ dimensional phase space for the four-segmented string. One of the constraints fixes the normalization of the spectral parameter, while the other six are equivalent to the constraints in (28). We have checked this explicitly for the 4-segmented string and (numerically) for the 6-segmented string. It is tempting to conjecture that the statement is also true for strings with an arbitrary number of segments.

References

- [1] K. Pohlmeyer, *Integrable Hamiltonian Systems and Interactions Through Quadratic Constraints*, *Commun. Math. Phys.* **46** (1976) 207–221.
- [2] R. Giles and C. B. Thorn, *Lattice approach to string theory*, *Phys. Rev. D* **16** (Jul, 1977) 366–386.
- [3] I. R. Klebanov and L. Susskind, *Continuum Strings From Discrete Field Theories*, *Nucl. Phys. B* **309** (1988) 175–187.
- [4] R. J. Baxter, *Partition function of the eight vertex lattice model*, *Annals Phys.* **70** (1972) 193–228.
- [5] R. J. Baxter, *Eight vertex model in lattice statistics and one-dimensional anisotropic Heisenberg chain. 1. Some fundamental eigenvectors*, *Annals Phys.* **76** (1973) 1–24.
- [6] Y. A. Antipov, *Diffraction of a plane wave by a circular cone with an impedance boundary condition*, *SIAM Journal on Applied Mathematics* **62** (2002), no. 4 1122–1152.
- [7] P. Hajicek, *Quantum mechanics of gravitational collapse*, *Commun. Math. Phys.* **150** (1992) 545–559.
- [8] V. Berezin, *Quantum black hole model and hawking’s radiation*, *Phys. Rev. D* **55** (Feb, 1997) 2139–2151.
- [9] J. M. Maldacena, *The large N limit of superconformal field theories and supergravity*, *Adv. Theor. Math. Phys.* **2** (1998) 231–252.
- [10] S. S. Gubser, I. R. Klebanov and A. M. Polyakov, *Gauge theory correlators from non-critical string theory*, *Phys. Lett.* **B428** (1998) 105–114 [[hep-th/9802109](#)].
- [11] E. Witten, *Anti-de Sitter space and holography*, *Adv. Theor. Math. Phys.* **2** (1998) 253–291.
- [12] J. A. Minahan and K. Zarembo, *The Bethe ansatz for $N=4$ superYang-Mills*, *JHEP* **03** (2003) 013 [[hep-th/0212208](#)].
- [13] I. Bena, J. Polchinski and R. Roiban, *Hidden symmetries of the $AdS(5) \times S^{*5}$ superstring*, *Phys. Rev.* **D69** (2004) 046002 [[hep-th/0305116](#)].
- [14] A. Cavaglià, N. Gromov, B. Stefański, Jr., Jr. and A. Torrielli, *Quantum Spectral Curve for AdS_3/CFT_2 : a proposal*, *JHEP* **12** (2021) 048 [[2109.05500](#)].

- [15] S. Ekhammar and D. Volin, *Monodromy bootstrap for $SU(2-2)$ quantum spectral curves: from Hubbard model to AdS_3/CFT_2* , *JHEP* **03** (2022) 192 [2109.06164].
- [16] N. Gromov, V. Kazakov, S. Leurent and D. Volin, *Quantum Spectral Curve for Planar $\mathcal{N} = 4$ Super-Yang-Mills Theory*, *Phys. Rev. Lett.* **112** (2014), no. 1 011602 [1305.1939].
- [17] N. Gromov, V. Kazakov, S. Leurent and D. Volin, *Quantum spectral curve for arbitrary state/operator in AdS_5/CFT_4* , *JHEP* **09** (2015) 187 [1405.4857].
- [18] N. Gromov, *Introduction to the Spectrum of $N = 4$ SYM and the Quantum Spectral Curve*, 1708.03648.
- [19] V. Kazakov, *Quantum Spectral Curve of γ -twisted $\mathcal{N} = 4$ SYM theory and fishnet CFT*, 1802.02160.
- [20] F. Levkovich-Maslyuk, *A review of the AdS/CFT Quantum Spectral Curve*, *J. Phys. A* **53** (2020), no. 28 283004 [1911.13065].
- [21] V. A. Fateev, S. L. Lukyanov and A. B. Zamolodchikov, *On mass spectrum in 't Hooft's 2D model of mesons*, *J. Phys. A* **42** (2009) 304012 [0905.2280].
- [22] N. Callebaut, S. S. Gubser, A. Samberg and C. Toldo, *Segmented strings in AdS_3* , *JHEP* **11** (2015) 110 [1508.07311].
- [23] A. Patrascioiu, *Quantum Dynamics of a Massless Relativistic String. 2.*, *Nucl. Phys. B* **81** (1974) 525–546.
- [24] W. A. Bardeen, I. Bars, A. J. Hanson and R. D. Peccei, *Study of the longitudinal kink modes of the string*, *Phys. Rev. D* **13** (Apr, 1976) 2364–2382.
- [25] X. Artru, *Classical String Phenomenology. 1. How Strings Work*, *Phys. Rept.* **97** (1983) 147.
- [26] B. Soederberg, B. Andersson and G. Gustafson, *Action-angle variables for the massless relativistic string in 1+1 dimensions*, *J Math Phys (NY)* **26(1)** (1985) 112–123.
- [27] A. Ficnar and S. S. Gubser, *Finite momentum at string endpoints*, *Phys. Rev.* **D89** (2014), no. 2 026002 [1306.6648].
- [28] J. C. Donahue and S. Dubovsky, *Confining Strings, Infinite Statistics and Integrability*, *Phys. Rev. D* **101** (2020), no. 8 081901 [1907.07799].

- [29] J. C. Donahue and S. Dubovsky, *Classical Integrability of the Zigzag Model*, *Phys. Rev. D* **102** (2020), no. 2 026005 [1912.08885].
- [30] J. C. Donahue and S. Dubovsky, *Quantization of the zigzag model*, *JHEP* **08** (2022) 047 [2202.11746].
- [31] S. S. Gubser, I. R. Klebanov and A. M. Polyakov, *A Semiclassical limit of the gauge / string correspondence*, *Nucl. Phys.* **B636** (2002) 99–114 [hep-th/0204051].
- [32] Y. B. Suris, *The Problem of Integrable Discretization: Hamiltonian Approach*. Birkhäuser Verlag, Basel, 2003.
- [33] D. Vegh, *The broken string in anti-de Sitter space*, *JHEP* **02** (2018) 045 [1508.06637].
- [34] D. Vegh, *Segmented strings from a different angle*, 1601.07571.
- [35] S. S. Gubser, *Evolution of segmented strings*, *Phys. Rev.* **D94** (2016), no. 10 106007 [1601.08209].
- [36] S. S. Gubser, S. Parikh and P. Witaszczyk, *Segmented strings and the McMillan map*, *JHEP* **07** (2016) 122 [1602.00679].
- [37] D. Vegh, *Segmented strings coupled to a B-field*, *JHEP* **04** (2018) 088 [1603.04504].
- [38] D. Vegh, *Pair-production of cusps on a string in AdS₃*, *JHEP* **03** (2021) 218 [1802.04306].
- [39] D. Vegh, *Celestial fields on the string and the Schwarzian action*, *JHEP* **07** (2021) 050 [1910.03610].
- [40] D. Vegh, *The spectral curve of segmented strings*, 2108.02674.
- [41] D. Vegh, *Segmented strings, brane tilings, and the Y-system*, 2112.14619.
- [42] A. Hanany and K. D. Kennaway, *Dimer models and toric diagrams*, hep-th/0503149.
- [43] S. Franco, A. Hanany, K. D. Kennaway, D. Vegh and B. Wecht, *Brane dimers and quiver gauge theories*, *JHEP* **01** (2006) 096 [hep-th/0504110].
- [44] A. Hanany and D. Vegh, *Quivers, tilings, branes and rhombi*, *JHEP* **10** (2007) 029 [hep-th/0511063].
- [45] B. Feng, Y.-H. He, K. D. Kennaway and C. Vafa, *Dimer models from mirror symmetry and quivering amoebae*, *Adv. Theor. Math. Phys.* **12** (2008), no. 3 489–545 [hep-th/0511287].

- [46] N. Arkani-Hamed, J. L. Bourjaily, F. Cachazo, A. B. Goncharov, A. Postnikov and J. Trnka, *Grassmannian Geometry of Scattering Amplitudes*. Cambridge University Press, 4, 2016.
- [47] M. Gekhtman, M. Shapiro, S. Tabachnikov and A. Vainshtein, *Integrable cluster dynamics of directed networks and pentagram maps*, *Advances in Mathematics* **300** (2016) 390–450. Special volume honoring Andrei Zelevinsky.
- [48] M. Gekhtman, M. Shapiro, S. Tabachnikov and A. Vainshtein, *Higher pentagram maps, weighted directed networks, and cluster dynamics*, 2012.
- [49] N. Dorey and B. Vicedo, *A Symplectic Structure for String Theory on Integrable Backgrounds*, *JHEP* **03** (2007) 045 [[hep-th/0606287](#)].
- [50] B. Vicedo, *The method of finite-gap integration in classical and semi-classical string theory*, *J. Phys. A* **44** (2011) 124002 [[0810.3402](#)].
- [51] E. K. Sklyanin, *Separation of Variables: New Trends*, *Progress of Theoretical Physics Supplement* **118** (01, 1995) 35–60 [[solv-int/9504001](#)].
- [52] S. Ruijsenaars and H. Schneider, *A new class of integrable systems and its relation to solitons*, *Annals of Physics* **170** (1986), no. 2 370–405.
- [53] H. W. Braden and R. Sasaki, *The Ruijsenaars-Schneider model*, *Prog. Theor. Phys.* **97** (1997) 1003–1018 [[hep-th/9702182](#)].
- [54] I. Aniceto and A. Jevicki, *N-body Dynamics of Giant Magnons in $R \times S^{*2}$* , [0810.4548](#).
- [55] K. R. Goncharov, Alexander B., *Dimers and cluster integrable systems*, *Annales scientifiques de l’Ecole Normale Supérieure* **46** (2013), no. 5 747–813.
- [56] G. ’t Hooft, *A Two-Dimensional Model for Mesons*, *Nucl. Phys. B* **75** (1974) 461–470.
- [57] G. Hooft, *A planar diagram theory for strong interactions*, *Nuclear Physics B* **72** (1974), no. 3 461–473.
- [58] R. C. Brower, W. L. Spence and J. H. Weis, *Bound States and Asymptotic Limits for QCD in Two-dimensions*, *Phys. Rev. D* **19** (1979) 3024.
- [59] S. Coleman, *Aspects of Symmetry: Selected Erice Lectures*. Cambridge University Press, 1985.

- [60] W. A. Bardeen, I. Bars, A. J. Hanson and R. D. Peccei, *Quantum Poincare Covariance of the $D = 2$ String*, *Phys. Rev. D* **14** (1976) 2193.
- [61] X. Artru, *Quantum noncovariance of the linear potential in $1 + 1$ dimensions*, *Phys. Rev. D* **29** (Mar, 1984) 1279–1280.
- [62] S. Lenz and B. Schreiber, *Example of a Poincare anomaly in relativistic quantum mechanics*, *Phys. Rev. D* **53** (1996) 960–966 [[hep-th/9503219](#)].
- [63] I. Bars and A. J. Hanson, *Quarks at the Ends of the String*, *Phys. Rev. D* **13** (1976) 1744–1760.
- [64] I. Bars, *A quantum string theory of hadrons and its relation to quantum chromodynamics in two dimensions*, *Nuclear Physics B* **111** (1976), no. 3 413–440.
- [65] Y. S. Kalashnikova and A. V. Nefediev, *$(1+1)$ string with quarks at the ends revisited*, *Phys. Lett. B* **399** (1997) 274–280 [[hep-th/9701193](#)].
- [66] R. Narayanan and H. Neuberger, *The Quark mass dependence of the pion mass at infinite N* , *Phys. Lett. B* **616** (2005) 76–84 [[hep-lat/0503033](#)].
- [67] Y. Li, P. Maris, X. Zhao and J. P. Vary, *Heavy Quarkonium in a Holographic Basis*, *Phys. Lett. B* **758** (2016) 118–124 [[1509.07212](#)].
- [68] L. D. Faddeev and G. P. Korchemsky, *High-energy QCD as a completely integrable model*, *Phys. Lett. B* **342** (1995) 311–322 [[hep-th/9404173](#)].
- [69] A. J. Hanson, R. Peccei and M. Prasad, *Two-dimensional $su(n)$ gauge theory, strings and wings: Comparative analysis of meson spectra and covariance*, *Nuclear Physics B* **121** (1977), no. 3 477–504.
- [70] R. F. Lebed and N. G. Uraltsev, *Precision studies of duality in the 't Hooft model*, *Phys. Rev. D* **62** (2000) 094011 [[hep-ph/0006346](#)].